ELSEVIER

Atherosclerosis 196 (2008) 391–397

ATHEROSCLEROSIS

www.elsevier.com/locate/atherosclerosis

A novel method for evaluating human carotid artery elasticity: Possible detection of early stage atherosclerosis in subjects with type 2 diabetes

Hisashi Okimoto[a,1], Yasushi Ishigaki[a,1], Yoshihiro Koiwa[b], Yoshinori Hinokio[a], Takehide Ogihara[c], Susumu Suzuki[a], Hideki Katagiri[c,f], Takayoshi Ohkubo[d,f], Hideyuki Hasegawa[e], Hiroshi Kanai[e], Yoshitomo Oka[a,g,*]

[a] *Division of Molecular Metabolism and Diabetes, Tohoku University Graduate School of Medicine, Japan*
[b] *Division of Cardiovascular Medicine, Tohoku University Graduate School of Medicine, Japan*
[c] *Division of Advanced Therapeutics for Metabolic Diseases, Tohoku University Graduate School of Medicine, Japan*
[d] *Department of Planning for Drug Development and Clinical Evaluation, Tohoku University Graduate School of Pharmaceutical Science and Medicine, Japan*
[e] *Department of Electrical Engineering, Tohoku University Graduate School of Engineering, Japan*
[f] *The 21st Century COE Programs, Comprehensive Research and Education Center for Planning of Drug Development and Clinical Evaluation, Japan*
[g] *The 21st Century COE Programs, Center for Innovative Therapeutic Development towards the Conquest of Signal Transduction Diseases, Tohoku University, Sendai, Japan*

Received 29 March 2006; received in revised form 5 September 2006; accepted 12 November 2006
Available online 18 December 2006

Abstract

We recently developed a novel method for evaluating the elasticity of arterial walls, the phased tracking method. Herein, we evaluated atherosclerosis of the carotid artery with this method in 242 individuals with type 2 diabetes. In multiple regression analysis of subject status, age, systolic blood pressure and hyperlipidemia were found to be independently associated with carotid artery elasticity values. We also measured currently established values for atherosclerosis, carotid artery IMT and baPWV, in these subjects. Carotid artery elasticity correlated with max IMT ($r=0.291$, $p<0.01$), plaque score (PS) ($r=0.220$, $p<0.01$) and baPWV ($r=0.345$, $p<0.01$). Elasticity, max IMT and plaque score, all correlated with the number of risk factors for atherosclerosis, i.e. hypertension, hyperlipidemia and smoking, in addition to diabetes, consistent with the view that these values reflect atherosclerosis. Importantly, however, in subjects with IMT <1.1 mm, who are classified as not having atherosclerosis as defined by IMT criteria, only carotid artery elasticity correlated with the number of risk factors ($p<0.05$). These results suggest that (1) the measured carotid artery elasticity values reflect atherosclerosis and (2) our novel method has potential for detecting atherosclerosis in its early stage.

Keywords: Human carotid artery elasticity; Atherosclerosis; Diabetes

1. Introduction

Individuals with type 2 diabetes are at very high risk for atherosclerosis [1]. Although many methods have been developed for detecting atherosclerosis, those currently available are mainly for detecting established atherosclerosis. Therefore, the disease process is well-advanced at the time of diagnosis. To reduce future cardiovascular complications in subjects with atherogenic disorders such as type 2 diabetes

* Corresponding author at: Division of Molecular Metabolism and Diabetes, Tohoku University Graduate School of Medicine, 2-1 Seiryo-machi, Aoba-ku, Sendai 980-8575, Japan. Tel.: +81 22 717 7611; fax: +81 22 717 7611.
E-mail address: oka-y@mail.tains.tohoku.ac.jp (Y. Oka).
[1] These authors contributed equally to this work.

0021-9150/$ – see front matter © 2006 Elsevier Ireland Ltd. All rights reserved.
doi:10.1016/j.atherosclerosis.2006.11.020

mellitus, detection of early stage atherosclerosis is urgently needed.

Carotid intima-media thickness (IMT) is a well-established surrogate marker for cardiovascular risk [2]. Measuring IMT with ultrasonography is non-invasive and relatively simple [3,4], and IMT is now commonly employed as an endpoint marker in clinical trials. Carotid IMT correlates with cardiovascular risk factors and indeed predicts macrovascular events such as myocardial infarction [5] and stroke [6]. Carotid IMT is greater in subjects with diabetes, both type 1 [7] and type 2 [8,9], than in non-diabetic subjects of the same age. When analyzed in diabetic patients, IMT correlates with glycemic control and the duration of diabetes. Interventions, such as blood glucose lowering [10], lipid lowering [11], ACE inhibition [12] and anti-platelet treatment [13], have been demonstrated to suppress IMT progression. However, it has also been reported that IMT is not affected by either therapeutic interventions [14] or glycemic control [15]. These conflicting results might be attributable to a very small change in IMT, a 0.1 mm increase per decade in normal subjects. Such a small change may mask actual change due to inter-assay variations in IMT measurement. Most importantly, it is not possible to make a diagnosis of atherosclerosis until the appearance of arterial wall thickening.

We recently developed a novel non-invasive method for evaluating the movement of multiple sites in cardiac and arterial walls (3.616 measurement sites/9.0 mm × 6.4 mm) during a single heartbeat [16,17]. This innovative phased tracking method enables us to evaluate regional characteristics; the softer the site, the more easily it deforms during one heartbeat. This reflects regional elasticity. This method has already been applied to the in vivo detection of regional changes in cardiac and arterial walls [18–20], and the interventricular septum [21]. Evaluation of plaque vulnerability has also been attempted [16]. It is theoretically possible to detect qualitative changes in the carotid arterial wall with this method. We therefore tested the possibility of being able to detect atherosclerosis in the early stage.

Herein, we show that carotid artery elasticity, as measured in Japanese subjects with type 2 diabetes, correlates well with results obtained with currently established methods for evaluating atherosclerosis. Most importantly, elasticity correlates with the number of risk factors for atherosclerosis in those with IMT <1.1 mm, who are classified as not having atherosclerosis as defined by IMT criteria [22,23]. These results strongly suggest that it is possible to detect early stage atherosclerosis with this novel method.

2. Methods

2.1. Study subjects

The study subjects were recruited from among patients followed at the diabetes clinic at Tohoku University Hospital. Patients with type 1 diabetes, renal failure (serum creatinine >2.0 mg/dl), severe heart failure (NYHA functional class 2–4), atrial fibrillation and peripheral arterial disease were excluded from the study. All participants analyzed were Japanese type 2 diabetes patients ($n = 242$) who met the WHO criteria for diabetes mellitus. The study protocol was approved by the Tohoku University Institutional Review Board. Informed consent was obtained from each patient. Subjects characteristics are shown in Table 1.

Table 1
Subject characteristics

Number	242
Age (years)	62.1 ± 12.4
Male (%)	54.1
Body weight (kg)	62.2 ± 13.6
BMI (kg/m^2)	24.2 ± 4.2
Duration of diabetes (years)	12.0 ± 9.70
Fasting blood glucose (mg/dl)	141 ± 32.1
HbA1c (%)	7.08 ± 1.33
Systolic blood pressure (mmHg)	130 ± 18.3
Diastolic blood pressure (mmHg)	75.8 ± 11.1
Total cholesterol (mg/dl)	191 ± 38.4
HDL cholesterol (mg/dl)	51.2 ± 14.6
LDL cholesterol (mg/dl)	115 ± 31.9
Triglyceride (mg/dl)	127 ± 94.1
Uric acid (mg/dl)	5.09 ± 1.37
High-sensitive CRP (mg/dl)	0.18 ± 0.23
Diabetic retinopathy (%)	30.2
Microalbumiuria or proteinuria (%)	38.8
Diabetic neuropathy (%)	46.4
Diet:OHA:insulin (%)	20.0:37.8:42.2
Hyperlipidemia (%)	37.2
Hypertension (%)	39.3
Current smoker (%)	30.6
BMI >25 (%)	38.0

Data are presented as means ± S.D.

We used the following criteria for atherogenic risk factors. Hyperlipidemia was defined as total cholesterol ≥5.7 mmol/dl (220 mg/dl) and/or triglyceride ≥1.7 mmol/l (150 mg/dl), based on the definition proposed by the Japan Atherosclerosis Society in 2002, or taking antihyperlipidemic drugs. The subjects whose systolic BP ≥140 mmHg and/or diastolic BP ≥90 mmHg (The Japanese Society of Hypertension guidelines in 2004) or who were taking antihypertensive drugs were defined as having hypertension. The subjects who currently smoked were classified as current smokers.

2.2. Measurement of ABI and baPWV

Ankle brachial pressure index (ABI) and brachial ankle pulse wave velocity (baPWV) were measured using an automatic waveform analyzer (BP-203RPE; Colin Co., Komaki, Japan) after a 5 min rest. This device was designed to simultaneously measure blood pressure levels in both arms (brachial arteries) and ankles (posterior tibial arteries), and to then calculate the ankle systolic BP/brachial systolic BP. Pulse waves were recorded on the right brachial artery and both posterior tibial arteries. The average baPWV was calculated by divid-

ing the arm–ankle distance by the pulse wave transmission time between these points.

2.3. Measurement of carotid artery intima-media thickness

Intima-media thickness of the carotid arteries was measured using ultrasound diagnostic equipment (EUB-450, Hitachi Medico, Tokyo, Japan) with an electrical linear transducer (mid-frequency of 7.5 MHz). The common carotid artery (CCA), carotid bulb and portions of the internal and external carotid arteries on both sides were scanned with the subject in the supine position. The scan encompasses the region between 30 mm proximal to the beginning of the dilation of the bifurcation bulb and 15 mm distal to the CCA flow divider. We defined the max IMT as the thickest IMT in the scanned regions [24] and a max IMT <1.1 mm was considered normal. We defined a plaque, a focal IMT thickening, as an area with IMT ≥1.1 mm and calculated the plaque score (PS) by totaling the maximal thickness values of all plaques in the scanned area [25]. The scans were performed by a trained sonographer and the scanning period averaged 20 min in each patient.

2.4. Measurement of arterial wall elasticity

Real-time measurement of regional elasticity in the carotid artery wall was achieved based on a previously described method [20] with ultrasound diagnostic equipment (prototype system by Panasonic). With this system, an ultrasound beam is used for sequential scanning at 32 positions with a linear type 7.5 MHz probe. Multiple points were preset from the luminal surface to the adventitia along each beam with constant intervals of 320 μm, and multiple layers were defined as being between two neighboring points. Then, the displacement of each point preset along each beam was obtained by applying the phased tracking method to the received echo. Minute changes in the thickness of each layer were determined by subtracting displacements of two neighboring points. The elasticity of each layer was obtained from the thickness change and the blood pressure measured at the upper arm. Since the reflected ultrasound was resampled at an interval of 107 ns (=80 μm along the depth direction) after quadrature demodulation, we further divided each layer with a thickness of 320 μm into four points, shifted the initial depth of each layer by one-fourth of 320 μm, and applied the above procedure to each depth. Thus, the elasticity was obtained at intervals of 80 μm in the depth direction and 200 μm in the axial direction of the artery. A cross-sectional image and the process of elasticity measurement are schematically depicted in Fig. 1.

2.5. Statistical analysis

Variables were compared using Pearson's regression analysis and Student's *t*-test as appropriate. Then, a multiple linear regression analysis was performed to evaluate the independent parameters that were significantly related to arterial elasticity. The relationships between number of risk factors and the values of atherosclerosis markers were examined by analysis of covariance (ANCOVA), adjusted with age as a covariate. A p value less than 0.05 was accepted as indicating statistical significance. All statistical analyses were performed using the Statistical Package for the Social Sciences Version 13.0 (SPSS Japan Inc., Tokyo, Japan).

3. Results

We assessed the associations of carotid artery elasticity with subject characteristics (Table 2). Elasticity correlated

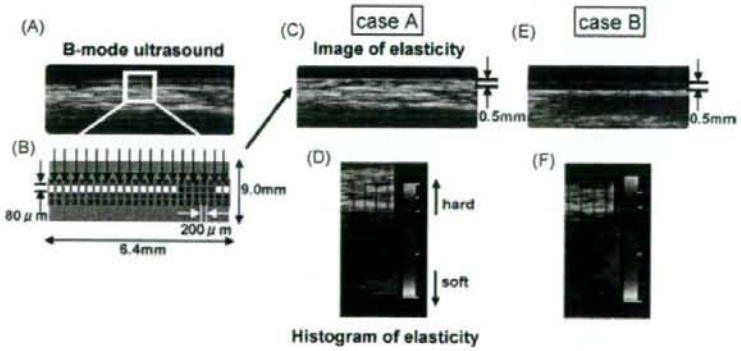

Fig. 1. The intima–media complex was visualized by conventional B-mode scanning (A), and minute thickness changes in the layers at each depth (113 depths × 32 beams per 9 mm × 6.4 mm scanned area) during one heart beat were then recorded by the phased tracking method (B). Thickness changes in each layer represent deformity, a reflection of elasticity. This elasticity is displayed as a 2D cross-sectional color image on B-mode scanning, and the image is updated at every heartbeat (C). The elasticity distribution is shown as a histogram (D). Representative results obtained from a normal subject, case A (male, age 40), are shown. Case B (male, age 45), in marked contrast, suffered from type 2 diabetes, hyperlipidemia and an old cerebral infarction, but had an IMT of only 0.5 mm, the same thickness as that of case A. The elasticity (E) was, however, extremely different from that of case A, as shown in the histogram (F).

Table 2
Associations between arterial elasticity and subject characteristics

Variables	r-Value	p-Value
Age	0.34	<0.01
Duration of diabetes	0.136	<0.05
Fasting blood glucose	−0.012	0.86
HbA1c	−0.003	0.97
Total cholesterol	0.103	0.10
HDL cholesterol	0.066	0.31
LDL cholesterol	0.089	0.17
Triglyceride	−0.064	0.32
Systolic blood pressure	0.443	<0.01
Diastolic blood pressure	0.147	<0.05
Uric acid	−0.03	0.65
High-sensitive CRP	0.037	0.56

Table 3
Mean arterial elasticity values in the presence and absence of cardiovascular risk factors

Variables	Elasticity (kPa)		p
	−	+	
Male	51.6 ± 12.6	51.0 ± 14.5	0.99
Hyperlipidemia	49.8 ± 12.3	54.7 ± 13.7	<0.01
Hypertension	49.6 ± 13.3	54.8 ± 13.6	<0.01
Current smoker	51.6 ± 13.3	51.8 ± 14.5	0.88
BMI >25	51.6 ± 13.7	51.6 ± 13.5	0.99
Diabetic retinopathy	52.3 ± 13.7	50.9 ± 14.1	0.67
Diabetic nephropathy	50.5 ± 13.6	53.9 ± 13.6	0.06
Diabetic neuropathy	50.8 ± 12.9	51.4 ± 14.4	0.65

Data are presented as means ± S.D.

Table 4
Multivariate adjustment for parameters related to arterial elasticity

Variables	Coefficient (β)	95% CI	p-Value
Age (years)	0.28	0.18–0.43	<0.01
Duration of diabetes (years)	−0.02	−0.18–0.14	0.77
Systolic blood pressure (mmHg)	0.39	0.21–0.38	<0.01
Hyperlipidemia	0.11	0.08–6.24	<0.05

with age ($r = 0.340$, $p < 0.01$), duration of diabetes ($r = 0.136$, $p < 0.05$) and blood pressure, both systolic ($r = 0.430$, $p < 0.01$) and diastolic ($r = 0.147$, $p < 0.05$).

We then examined whether or not cardiovascular risk factors affect arterial elasticity values (Table 3). Hyperlipidemic subjects had significantly higher arterial elasticity values than those with normal lipid profiles. Similarly, subjects with hypertension had higher values. However, arterial elasticity values did not depend on other risk factors, such as sex, obesity, smoking and diabetic complications.

To elucidate the independent variables affecting arterial elasticity, we performed multiple linear regression analysis with parameters related to elasticity. We employed four clinical parameters, age, duration of diabetes, systolic blood pressure and hyperlipidemia, based on the results shown in Tables 2 and 3. We found age, systolic blood pressure and hyperlipidemia to be independently associated with elasticity values (Table 4).

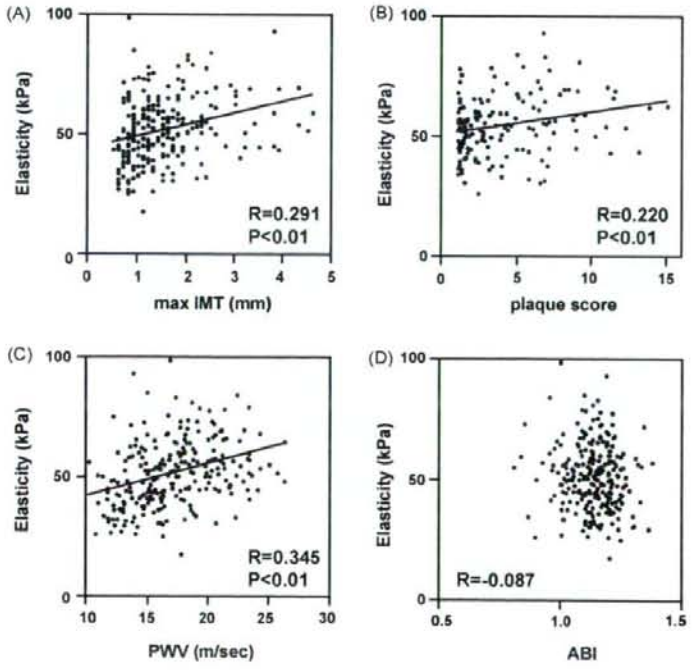

Fig. 2. Correlations between arterial elasticity values and max IMT (A), plaque score (B), baPWV (C) and ABI (D).

To assess the clinical relevance of carotid artery elasticity, we compared our elasticity values to those obtained with currently established methods for evaluating atherosclerosis: max IMT, plaque score, baPWV and ABI. Carotid artery elasticity showed significant positive correlations with max IMT ($r=0.291$, $p<0.01$) (Fig. 2A), the plaque score ($r=0.220$, $p<0.01$, $n=160$) (Fig. 2B) and baPWV ($r=0.345$, $p<0.01$) (Fig. 2C) in subjects with type 2 diabetes. It should be kept in mind that the plaque score can be obtained only in subjects with IMT $\geq$1.1 mm ($n=160$), such that the correlation was studied only in those having definite atherosclerosis based on IMT criteria [22,23]. Arterial elasticity showed no correlation with the ABI value ($r=-0.087$, $p=0.176$) (Fig. 2D). However, when we performed multiple linear regression analysis adjusted with independent parameters, age, systolic blood pressure and hyperlipidemia (Table 4), the correlations between elasticity and atherosclerosis markers (max IMT, plaque score and baPWV) were no longer present.

In a subject with more than one risk factor, the atherosclerotic process would be accelerated and thus affect the values of atherosclerosis markers. Four modifiable risk factors, diabetes, hypertension, hyperlipidemia and current smoking,

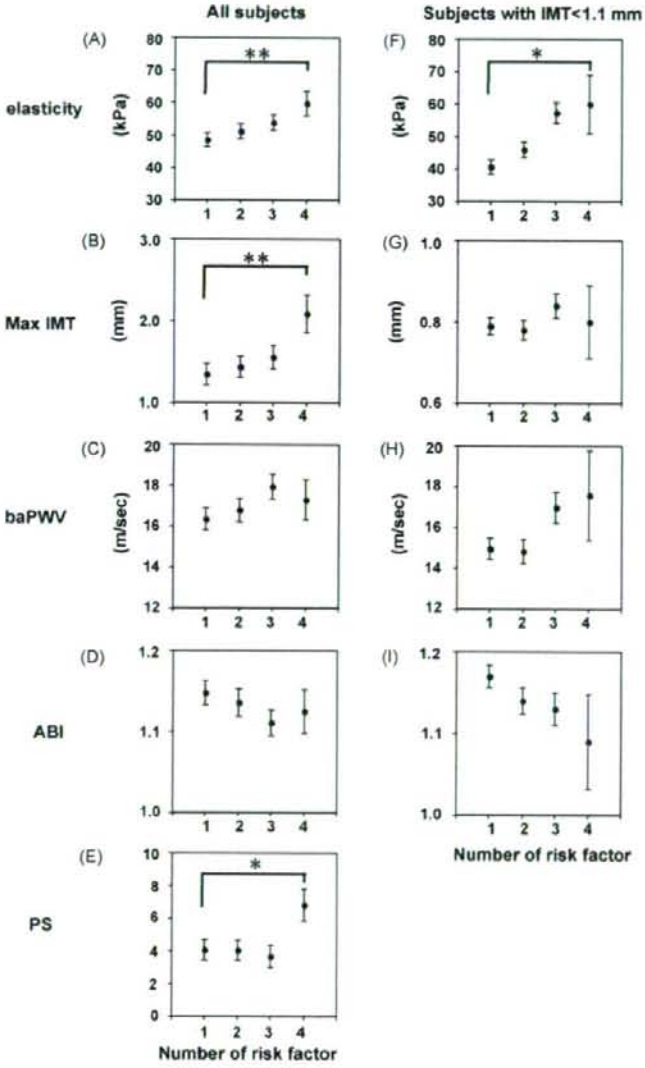

Fig. 3. Correlations of values reflecting atherosclerosis with the number of risk factors in all study subjects (A–E, $n=242$) and subjects with max IMT <1.1 mm (F–I, $n=82$). Data are presented as means ± S.E. $^{*}p<0.05$, $^{**}p<0.01$.

were taken into account in this study. All subjects had at least one risk factor, diabetes. When all the subjects were analyzed by ANCOVA, adjusted with age as a covariate, the higher the number of risk factors, the greater the attenuation of arterial elasticity values, max IMT and the plaque score (Fig. 3A, B, E). However, very interestingly, when subjects with max IMT <1.1 mm, who are regarded as not having atherosclerosis based on IMT criteria, were analyzed ($n = 82$), only age-adjusted carotid artery elasticity correlated with an increasing number of risk factors (Fig. 3F). Other age-adjusted parameters for evaluating atherosclerosis, max IMT, baPWV and ABI, showed no significant correlations with a greater number of risk factors in subjects with max IMT <1.1 mm (Fig. 3G–I).

4. Discussions

Our most important finding is that in subjects with max IMT <1.1 mm, who are regarded as being free of atherosclerosis based on IMT criteria [22,23], only carotid artery elasticity as measured with our novel non-invasive method correlated with an increasing number of risk factors. No other values obtained with the currently available methods showed correlations with the number of risk factors in these "non-atherosclerotic" subjects. Thus, our novel method of measuring arterial wall elasticity raises the possibility of detecting atherosclerosis in its early stage.

Carotid artery elasticity correlates well with results obtained with currently established methods for evaluating atherosclerosis in subjects with type 2 diabetes. These results strongly suggest that elasticity as measured with our current method reflects the severity of atherosclerosis. The measurement procedures are relatively simple, essentially the same as those of B-mode ultrasonography. In addition, arterial wall elasticity is shown as a color coded cross-sectional image with a side by side B-mode ultrasonogram, which is very practical in the clinical setting.

This novel ultrasonic method accurately tracks the movement of the arterial wall based on both the phase and the magnitude of demodulated signals, allowing instantaneous determination of the position of an object. With this method, it is possible to accurately detect small-amplitude velocity signals, less than a few micrometers, that are superimposed on arterial wall motion due to the heartbeat. This method thus allows the elasticity, a qualitative feature, of the arterial wall to be evaluated. In addition to detecting the early stage atherosclerosis, this method may enable us to evaluate progression or regression of atherosclerosis in a much shorter time than currently available methods. This possibility is extremely interesting because a means of evaluating whether or not a treatment is effective for preventing atherosclerosis is urgently needed. It usually takes years to detect the progression or regression of atherosclerosis, while it may take only months with our present method of qualitative arterial wall measurement. For example, it may be possible to detect an improvement in response to statin treatment within a few months. Similarly, we will be able to assess the effects on atherosclerosis of altering risk factors within months. These possibilities clearly merits further study.

A variety of methods are widely used for evaluating atherosclerosis. Measuring carotid IMT with ultrasound is one of the most well-established methods because it is safe, non-invasive, reproducible and easy to perform. IMT provides quantitative information, i.e. vessel-wall thickness. Depicting changes in IMT is thus generally thought to take a long time. baPWV is also a non-invasive method, which assesses atherosclerosis, as a reflection of arterial stiffness, and the usefulness of baPWV has been reported in clinical studies [26–28]. However, the pulse wave velocity depends on the ratio of the inner radius of the artery to wall thickness, which is not related to regional elasticity. It also reportedly depends on heart rate [29].

While the elasticity average of the intima and media of the carotid artery wall was calculated and used for evaluation of atherosclerosis in this study, another interesting aspect of elasticity is its distribution. The elasticity distribution, which is depicted in a histogram, might provide additional information regarding qualitative changes in atherosclerosis, and should be comprehensively studied in the future. In conclusion, our novel method for evaluating carotid artery wall elasticity holds promise for early detection of atherosclerosis.

Acknowledgments

This work was supported by a Grant-in-Aid for Scientific Research (17790599) to Y. Ishigaki and the 21st Century COE Programs "Innovative Therapeutic Development towards the Conquest of Signal Transduction Diseases" to Y. Oka from the Ministry of Education, Science, Sports and Culture of Japan. This work was also supported by a Grant-in-Aid for Research on Human Genome, Tissue Engineering (H17-genome-003) to Y. Oka. We thank Healthcare Business Company, Matsushita Electric Industrial Co., Ltd. (Panasonic), Yokohama, Japan for supplying the prototype elasticity measurement system for this study.

References

[1] Kannel WB, McGee DL. Diabetes and cardiovascular disease. The Framingham study. JAMA 1997;241:2035–8.
[2] O'Leary DH, Polak JF, Kronmal RA, et al. Carotid-artery intima and media thickness as a risk factor for myocardial infarction and stroke in older adults. Cardiovascular Health Study Collaborative Research Group. N Engl J Med 1999;340:14–22.
[3] Pignoli P, Tremoli E, Poli A, Oreste P, Paoletti R. Intimal plus medial thickness of the arterial wall: a direct measurement with ultrasound imaging. Circulation 1986;74:1399–406.
[4] Salonen JT, Korpela H, Salonen R, Nyyssonen K. Precision and reproducibility of ultrasonographic measurement of progression of common carotid artery atherosclerosis. Lancet 1993;341:1158–9.

[5] Bots ML, Hoes AW, Koudstaal PJ, Hofman A, Grobbee DE. Common carotid intima-media thickness and risk of stroke and myocardial infarction: the Rotterdam Study. Circulation 1997;96:1432–7.
[6] Touboul PJ, Elbaz A, Koller C, et al. Common carotid artery intima-media thickness and brain infarction: the Etude du Profil Genetique de l'Infarctus Cerebral (GENIC) case-control study. The GENIC Investigators. Circulation 2000;102:313–8.
[7] Yamasaki Y, Kawamori R, Matsushima H, et al. Atherosclerosis in carotid artery of young IDDM patients monitored by ultrasound high-resolution B-mode imaging. Diabetes 1994;43:634–9.
[8] Folsom AR, Eckfeldt JH, Weitzman S, et al. Relation of carotid artery wall thickness to diabetes mellitus, fasting glucose and insulin, body size, and physical activity. Atherosclerosis Risk in Communities (ARIC) Study Investigators. Stroke 1994;25:66–73.
[9] Kawamori R, Yamasaki Y, Matsushima H, et al. Prevalence of carotid atherosclerosis in diabetic patients. Ultrasound high-resolution B-mode imaging on carotid arteries. Diabetes Care 1992;15:1290–4.
[10] Minamikawa J, Tanaka S, Yamauchi M, Inoue D, Koshiyama H. Potent inhibitory effect of troglitazone on carotid arterial wall thickness in type 2 diabetes. J Clin Endocrinol Metab 1998;83:1818–20.
[11] Furberg CD, Adams Jr HP, Applegate WB, et al. Effect of lovastatin on early carotid atherosclerosis and cardiovascular events. Asymptomatic Carotid Artery Progression Study (ACAPS) Research Group. Circulation 1994;90:1679–87.
[12] Lonn E, Yusuf S, Dzavik V, et al. Effects of ramipril and Vitamin E on atherosclerosis: the study to evaluate carotid ultrasound changes in patients treated with ramipril and Vitamin E (SECURE). Circulation 2001;103:919–25.
[13] Kodama M, Yamasaki Y, Sakamoto K, et al. Antiplatelet drugs attenuate progression of carotid intima-media thickness in subjects with type 2 diabetes. Thromb Res 2000;97:239–45.
[14] Beishuizen ED, van de Ree MA, Jukema JW, et al. Two-year statin therapy does not alter the progression of intima-media thickness in patients with type 2 diabetes without manifest cardiovascular disease. Diabetes Care 2004;27:2887–92.
[15] Rantala AO, Paivansalo M, Kauma H, et al. Hyperinsulinemia and carotid atherosclerosis in hypertensive and control subjects. Diabetes Care 1998;21:1188–93.
[16] Kanai H, Hasegawa H, Ichiki M, Tezuka F, Koiwa Y. Elasticity imaging of atheroma with transcutaneous ultrasound: preliminary study. Circulation 2003;107:3018–21.
[17] Hasegawa H, Kanai H, Hoshimiya N, Koiwa Y. Evaluating the regional elastic modules of a cylindrical shell with nonuniform wall thickness. J Med Ultrason 2004;31:81–90.
[18] Kanai H, Sato M, Koiwa Y, Chubachi N. Transcutaneous measurement and spectrum analysis of heart wall vibrations. IEEE Trans Ultrason Ferroelectr Freq Control 1996;43:791–810.
[19] Kanai H, Koiwa Y, Zhang J. Real-time measurement of local myocardium motion and arterial wall thickening. IEEE Trans Ultrason Ferroelectr Freq Control 1999;46:1229–41.
[20] Hasegawa H, Kanai H, Hoshimiya N, Chubachi N, Koiwa Y. Accuracy evaluation in the measurement of a small change in the thickness of arterial walls and the measurement of elasticity of the human carotid artery. Jpn J Appl Phys 1998;37:3101–5.
[21] Kanai H, Hasegawa H, Chubachi N, Koiwa Y, Tanaka M. Noninvasive evaluation of local myocardinal thickening and its color-coded imaging. IEEE Trans Ultrason Ferroelectr Freq Control 1997;44:752–68.
[22] Salonen R, Seppanen K, Rauramaa R, Salonen JT. Prevalence of carotid atherosclerosis and serum cholesterol levels in eastern Finland. Arteriosclerosis 1988;8:788–92.
[23] Poli A, Tremoli E, Colombo A, et al. Ultrasonographic measurement of the common carotid artery wall thickness in hypercholesterolemic patients. A new model for the quantitation and follow-up of preclinical atherosclerosis in living human subjects. Atherosclerosis 1988;70:253–61.
[24] O'Leary DH, Polak JF, Kronmal RA, et al. Distribution and correlates of sonographically detected carotid artery disease in the Cardiovascular Health Study. The CHS Collaborative Research Group. Stroke 1992;23:1752–60.
[25] Handa N, Matsumoto M, Maeda H, et al. Ultrasonic evaluation of early carotid atherosclerosis. Stroke 1990;21:1567–72.
[26] Lehmann ED, Hopkins KD, Gosling RG. Increased aortic stiffness in women with NIDDM. Diabetologia 1996;39:870–1.
[27] Farrar DJ, Green HD, Wagner WD, Bond MG. Reduction in pulse wave velocity and improvement of aortic distensibility accompanying regression of atherosclerosis in the rhesus monkey. Circ Res 1980;47:425–32.
[28] Lehmann ED, Riley WA, Clarkson P, Gosling RG. Non-invasive assessment of cardiovascular disease in diabetes mellitus. Lancet 1997;350(Suppl. 1):SI14–9.
[29] Lantelme P, Mestre C, Lievre M, Gressard A, Milon H. Heart rate: an important confounder of pulse wave velocity assessment. Hypertension 2002;39:1083–7.

Am J Physiol Endocrinol Metab 294: E668–E678, 2008.
First published January 29, 2008; doi:10.1152/ajpendo.00640.2007.

Ambient glucose levels qualify the potency of insulin myogenic actions by regulating SIRT1 and FoxO3a in C_2C_{12} myocytes

Taku Nedachi,[1] Akito Kadotani,[1,3] Miyako Ariga,[1,2] Hideki Katagiri,[2,3] and Makoto Kanzaki[1,4]

[1]*Division of Biomaterials, Tohoku University Biomedical Engineering Research Organization;* [2]*21st COE program "CRESCENDO", Graduate School of Pharmaceutical Sciences;* [3]*Division of Advanced Therapeutics for Metabolic Diseases, Center for Translational and Advanced Animal Research; and* [4]*Center for Research Strategy and Support, Tohoku University, Sendai, Japan*

Submitted 3 October 2007; accepted in final form 18 January 2008

Nedachi T, Kadotani A, Ariga M, Katagiri H, Kanzaki M. Ambient glucose levels qualify the potency of insulin myogenic actions by regulating SIRT1 and FoxO3a in C_2C_{12} myocytes. *Am J Physiol Endocrinol Metab* 294: E668–E678, 2008. First published January 29, 2008; doi:10.1152/ajpendo.00640.2007.—Nutrition availability is one of the major environmental signals influencing cell fate, such as proliferation, differentiation, and apoptosis, often functioning in concert with other humoral factors, including insulin. Herein, we show that low-serum-induced differentiation of C_2C_{12} myocytes is significantly hampered under low glucose (LG; 5 mM) compared with high glucose (HG; 22.5 mM) conditions, concurrently with nuclear accumulation of SIRT1, an NAD^+-dependent deacetylase, and FoxO3a, both of which are implicated in the negative regulation of myogenesis. Intriguingly, insulin appears to exert opposite actions, depending on glucose availability, with regard to the regulation of SIRT1 and FoxO3a abundance, which apparently contributes to modulating the potency of insulin's myogenic action. Namely, insulin exerts a potent myogenic effect in the presence of sufficient glucose, whereas insulin is unable to exert its myogenic action under LG conditions, since insulin evokes massive upregulation of both SIRT1 and FoxO3a in the absence of sufficient ambient glucose. In addition, the hampered differentiation state under LG is significantly restored by sirtinol, a SIRT1 inhibitor, whereas insulin abolished this sirtinol-dependent restoration, indicating that insulin can function as a negative as well as a positive myogenic factor depending on glucose availability. Taken together, our data reveal the importance of ambient glucose levels in the regulation of myogenesis and also in the determination of insulin's myogenic potency, which is achieved, at least in part, through regulation of the cellular contents and localization of SIRT1 and FoxO3a in differentiating C_2C_{12} myocytes.

forkhead box O; differentiation

SKELETAL MUSCLE CELLS have provided a useful model for exploring the molecular mechanisms involved in cellular differentiation (13), and insulin and insulin-like growth factors (IGFs) have been implicated in the process of myogenesis by activating the IRS-PI 3-kinase signaling pathway (7, 22, 25, 53) that also serves as a pivotal intracellular signal for exerting metabolic actions in mature skeletal muscle (9). However, despite our general understanding of the effects of ambient glucose levels on insulin responsiveness with regard to metabolic actions in skeletal muscle cells (37), the possible interrelationship between glucose and insulin acting on myogenesis remains to be clarified.

Skeletal muscle differentiation is a well-organized process governed by muscle-specific transcription factors belonging to the MyoD family, such as MyoD and myogenin (42), and the myocyte enhancer factor-2 (MEF2) family, such as MEF2A and MEF2C (35). In addition to these muscle-specific transcription factors, positively regulating myogenesis, the forkhead box O (FoxO) class of transcription factors, ubiquitously expressed in various cell types, has been shown to negatively regulate myogenesis (27). Insulin/IGF-induced repression of FoxO transcription factors, resulting from their nuclear exclusion in response to Akt-mediated phosphorylation, has been implicated in a key aspect of insulin/IGF actions not only for stimulating myogenesis but also for preventing muscle atrophy (21, 46).

Myogenesis is also directly influenced by the acetylation status of histones and nonhistone proteins including MyoD and MEF2, and class I and II histone deacetylases (HDACs) have been shown to regulate muscle gene expression by inhibiting MyoD and MEF2 factors (31, 33, 43). Recently, silent information regulator-2 (Sir2), a class III deacetylase originally characterized as controlling the life spans of animals in response to nutritional availability, was also identified to serve as a key regulator for myogenesis (14) via overexpression of SIRT1, the mammalian ortholog for Sir2, in C_2C_{12} myoblasts by strongly inhibiting differentiation into myotubes, whereas suppression of SIRT1 expression by RNA interference enhanced myogenesis (14).

Given the unique property of SIRT1 that the cofactor nicotinamide adenine dinucleotide (NAD^+) drives deacetylation activity, SIRT1 has been thought to serve as an energy and/or oxidation sensor, being directly involved in the nutritional regulation of gene transcription events in various tissues including skeletal muscle (38, 40, 45). Intriguingly, recent studies have also demonstrated that SIRT1 controls cellular functions by deacetylating FoxO transcription factors in response to various stimuli including nutritional availability (4, 36, 38). Thus, myogenesis is likely to be regulated cooperatively by SIRT1 serving as a sensor of the nutritional environment in concert with FoxOs serving as an insulin/IGF sensor in various situations in which glucose and insulin levels are fluctuating. However, no data are available on the potential interplay between ambient glucose levels and insulin in the regulations of SIRT1 and FoxOs, or on the regulation of myogenesis.

Address for reprint requests and other correspondence: M. Kanzaki, Center for Research Strategy and Support (CRESS), Tohoku University, 2-1 Seiryo-machi, Aoba-ku, Sendai 980-8575, Japan (e-mail: Kanzaki@tubero.tohoku.ac.jp).

The costs of publication of this article were defrayed in part by the payment of page charges. The article must therefore be hereby marked "*advertisement*" in accordance with 18 U.S.C. Section 1734 solely to indicate this fact.

To gain insight into these issues, we investigated the effects of ambient glucose levels on differentiation of C_2C_{12} myocytes and found the potency of insulin's myogenic action to be remarkably affected by extracellular glucose levels and that insulin exerts its maximum myogenic effect only in the presence of a relatively high level of glucose, whereas its potency is significantly compromised under low glucose (LG) conditions, a state in which massive upregulations of SIRT1 and FoxO3a are induced by insulin treatment. Thus, these findings reveal an important interplay between ambient glucose and insulin favoring alterations in the cellular contents of SIRT1 and FoxO3a, both of which are tightly coupled to the regulation of myogenesis.

MATERIALS AND METHODS

Materials. The Western blot detection kit (West super femto detection reagents) was obtained from Pierce Biotechnology (Rockford, IL). Dulbecco's modified Eagle's medium (DMEM), penicillin-streptomycin and trypsin-EDTA were purchased from Sigma Chemicals (St. Louis, MO). Cell culture equipment was from BD Biosciences (San Jose, CA). Calf serum (CS) and fetal bovine serum (FBS) were obtained from BioWest (Nuaille, France). Immobilon-P and anti-SIRT1 antibody were from Millipore (Bedford, MA). Anti-myosin heavy chain (MHC; MF20) and anti-myogenin (F5D) antibodies were obtained from Iowa Hybridoma Bank (University of Iowa, Iowa City, IA). Anti-phospho-S6 ($Ser^{235/236}$), anti-Akt, anti-phospho-Akt (Ser^{473}), and anti-phospho Akt (Thr^{308}) antibodies were purchased from Cell Signaling Technology (Danvers, MA). Anti-β-actin antibody was obtained from Sigma Chemicals. Unless otherwise noted, all chemicals were of the purest grade available from Sigma Chemicals.

Cell culture. Mouse skeletal muscle cell line C_2C_{12} myoblasts (54) were maintained in DMEM supplemented with 10% FBS, 30 μg/ml penicillin, and 100 μg/ml streptomycin (growth medium) at 37°C under a 5% CO_2 atmosphere. For biochemical study, the cells were grown on 4-well plates (Nalgen Nunc International, Rochester, NY) at a density of 1×10^5 cells/well in 5 ml of growth medium or on 6-well plates (BD Biosciences) at a density of 3×10^4 cells/well in 3 ml of growth medium. Three days after plating, cells had reached ~80–90% confluence (*day 0*). Differentiation was then induced by switching the growth medium to DMEM supplemented with 2% CS, 30 μg/ml penicillin, and 100 μg/ml streptomycin (differentiation medium). The differentiation medium was changed every 24 h. For the immunofluorescent staining study, cells were grown on 22-mm glass coverslips (C022221; Matsunami, Osaka, Japan) in 6-well plates.

Immunofluorescent studies. C_2C_{12} myoblasts were cultured on coverslips placed on 6-well plates. After differentiation, the cells were stimulated with 100 nM insulin for 60 min. Then, the cells were fixed with 2% paraformaldehyde in PBS (without Ca^{2+} and Mg^{2+}), followed by immunocytochemistry using anti-SIRT1 antibody (Millipore), and anti-mouse IgG antibody conjugated with Alexa 555 or Alexa 594 (Invitrogen, Carlsbad, CA). Images were monitored and analyzed using Olympus Fluoview FV1000 confocal microscopy and the associated application program, ASW v. 1.3 (Olympus, Tokyo, Japan).

Nuclear extract preparation. Nuclear extract preparation was performed as follows. Briefly, the cells were washed three times with PBS (-) and resuspended in *buffer A* (10 mM HEPES-OH, pH 7.9, 1.5 mM $MgCl_2$, 10 mM KCl). After a 20-min incubation on ice, the cells were destroyed with a vortex mixer (maximum speed), and the pellets were then collected. The pellets were resuspended in 50 μl of *buffer C* (HEPES-OH, pH 7.9, 420 mM NaCl, 1.5 mM $MgCl_2$, 0.2 mM EDTA, 25% glycerol) and then frozen (−80°C) and thawed twice. The supernatants were collected as nuclear extracts, and the protein concentration was measured and then stored at −80°C until Western blot analysis.

Immunoprecipitation. The cell lysates were prepared using Triton X-100-NP40 lysis buffer (50 mM Tris-Cl, 150 mM NaCl, 1 mM EDTA, 1% Triton X-100, 1% NP-40) and the protein concentrations of each sample were measured using a bicinchoninic acid assay (BCA) protein assay kit (Pierce). Five hundred micrograms of protein were mixed with 2 μg of anti-SIRT1 polyclonal antibody. The mixtures were incubated at 4°C for 3 h and continuously incubated in the presence of protein A-Sepharose. The immunoprecipitates were washed with Triton X-100-NP-40 lysis buffer three times. The adsorbed proteins were eluted with 1× Laemmli's buffer, boiled, and subjected to Western blot analysis.

Western blot analysis. The expression and phosphorylation of each protein were analyzed by Western blot analysis. In brief, the harvested cell lysates were subjected to 5% or 12% SDS-polyacrylamide gel electrophoresis (1:30 bis:acrylamide). Proteins were transferred to a PVDF membrane (Immobilon-P, Millipore), and the membranes were then blocked for 2 h at room temperature with 5% nonfat dry milk in Tris-buffered saline (TBS) containing 0.1% Tween-20. Immunostaining to detect each protein was achieved with a 1-h incubation with a 1:1,000 dilution of anti-SIRT1 antibody, anti-myosin heavy chain antibody, and anti-myogenin antibody. Specific totals or phosphoproteins were visualized after subsequent incubation with a 1:5,000 dilution of anti-mouse or rabbit IgG conjugated to horseradish peroxidase and a SuperSignal chemiluminescence detection procedure (Pierce Biotechnology). Protein concentrations were determined using a BCA assay. Three independent experiments were performed for each condition. Coomassie blue staining was also performed to assess the efficiency of protein transfer.

Real-time PCR. Fluorescence real-time PCR analysis was performed using a Light Cycler instrument and SYBR Green detection kit according to the manufacturer's instructions (Roche Diagnostics, Indianapolis, IN). PCR primers for measuring each of the secreted factors were as follows: for SIRT1, 5′-GAT CCT TCA GTG TCA TGG TT-3′ and 5′-GAA GAC AAT CTC TGG CTT CA-3′; for FoxO3a, 5′-TGC CTT GTC AAA TTC TGT C-3′ and 5′-TGC ACT AGC TGA ATA CAG TGA G-3′; for GAPDH, 5′-GGA GAA ACC TGC CAA GTA TGA-3′ and 5′-GCA TCG AAG GTG GAA GAG T-3′.

Glucose concentration assay. Glucose concentrations in the cultured media were measured using a determiner GLE kit (Kyowa Medex, Tokyo, Japan).

Statistical analysis. Statistical analysis was performed using one-way ANOVA followed by Tukey's multiple comparison test or Student's paired *t*-test for independent samples. Data are expressed as means ± SE unless otherwise specified.

RESULTS

Extracellular glucose influences low-serum-induced C_2C_{12} differentiation. To characterize the effects of extracellular glucose levels on myogenesis of C_2C_{12} cells, we first examined whether the glucose concentration in the low-serum differentiation medium (DMEM + 2% CS) affects C_2C_{12} differentiation. Under the LG (5 mM glucose) conditions, the process of myogenesis was obviously delayed and the number of well-developed myotubes was decreased compared with high glucose (22.5 mM glucose; HG) conditions on *day 4* of differentiation (Fig. 1*A*). We quantified differentiation status by counting the number of myotubes defined as multinuclear myotubes that contained more than 5 nuclei (Fig. 1*B*), as we previously reported (37). The effect of the extracellular glucose concentration on myogenesis was confirmed by Western blot analysis of differentiation marker proteins using anti-skeletal muscle type MHC and anti-myogenin antibodies, as not only were their expressions detected later, but their amounts were also

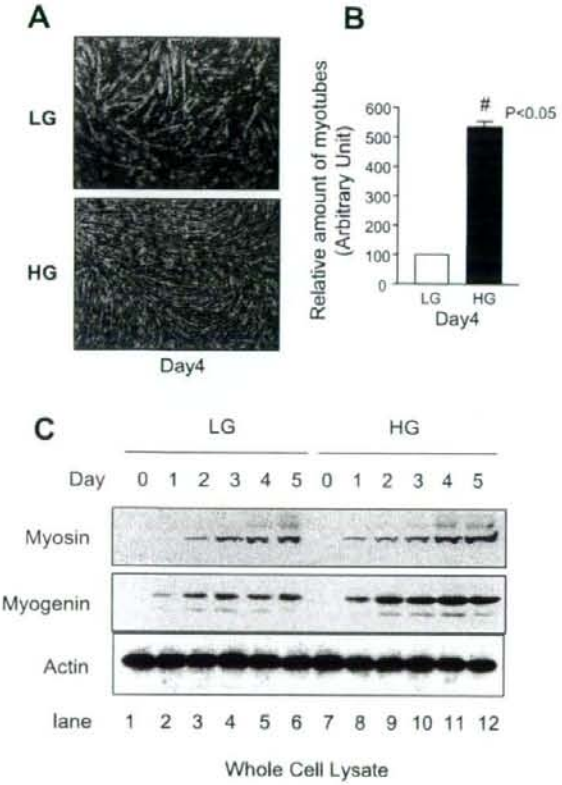

Fig. 1. Low-serum-induced C_2C_{12} myoblast differentiation was affected by extracellular glucose levels. *A* and *B*: C_2C_{12} myoblasts were cultured in low glucose (LG)-DMEM (5 mM glucose) + 10% FBS and then switched to differentiation medium [DMEM + 2% calf serum (CS); D-medium] containing 5 mM (LG) or 22.5 mM high glucose (HG) glucose (*day 0*). Cells were continuously cultured with D-medium changes every 24 h. *A*: at *day 4* of differentiation under LG (*a*) or HG (*b*) conditions, myotube formations were observed under a microscope. *B*: relative numbers of myotubes, defined as multinuclear myotubes containing more than 5 nuclei, were determined. Statistical analysis was performed using paired *t*-test. #$P < 0.05$ ($n = 5$). *C*: on the indicated day, cell lysates were prepared, and the same amounts of proteins were subjected to Western blotting using anti-myosin, anti-myogenin, and anti-β-actin antibodies. Each experiment was repeated 3 times and representative results are shown.

lower than in C_2C_{12} cells differentiated under LG conditions (Fig. 1*C*).

SIRT1 predominantly localizes in the nucleus under LG conditions but is excluded under HG conditions in C_2C_{12} myotubes. To understand the mechanisms by which extracellular glucose alters the process of C_2C_{12} differentiation, we initially focused on SIRT1, an NAD-dependent protein deacetylase with enzymatic activity sensitive to changes in cellular energy levels (for a review, see Ref. 2), since a recent study showed direct involvement of SIRT1 in myogenesis (14). Consistent with previous reports showing that Sir2 and its mammalian homolog SIRT1 are localized in the nucleus (19, 34), immunofluorescent analysis using anti-SIRT1 antibody demonstrated that, when C_2C_{12} cells were differentiated under LG conditions, predominant localization of SIRT1 was observed in the nucleus (Fig. 2*A*, *a*) similar to what was observed in undifferentiated myoblasts (data not shown). In contrast, when C_2C_{12} myoblasts were differentiated under HG conditions, the number of SIRT1-positive nuclei was remarkably reduced (Fig. 2*A*, *c*, see arrowheads), as confirmed by Western blotting analysis of nuclear proteins extracted under each culture condition (data not shown). Counterstaining was performed with DAPI (Fig. 2*A*, *b* and *d*). Immunofluorescent analysis demonstrated that the nuclear exclusion of SIRT1 was not acutely induced by HG administration in either myoblasts (data not shown) or LG-differentiated myotubes (Fig. 2*B*). However, we found that total SIRT1 protein was significantly reduced when C_2C_{12} cells were differentiated under HG conditions (Fig. 2*C*, *bottom*, HG-SIRT1) compared with those under LG conditions (*top*, LG-SIRT1). The HG-dependent reduction of SIRT1 was obvious from *day 2* of differentiation (Fig. 2*C*, *bottom*, HG-SIRT1, *lane3*).

Myogenesis is a highly organized and regulated sequence of multiple processes orchestrated by a wide variety of functional proteins, including SIRT1, requiring a relatively long time, and all of these processes could be affected by ambient glucose levels. In an attempt to dissect the effects of glucose on SIRT1 regulation and myogenesis, we conducted an experiment to specify the time required for glucose to exert its effect on SIRT1 suppression. Thus, C_2C_{12} myotubes differentiated under LG conditions (*days 5–6*) were transferred to HG or the same LG medium, and time course changes in SIRT1 contents were analyzed by Western blotting (Fig. 2, *D* and *E*). The time course experiment revealed that 24-h exposure to HG is sufficient for reducing the cellular SIRT1 content and its nuclear localization (data not shown) in LG-differentiated C_2C_{12} myotubes. In addition, we performed the converse experiments; that is, C_2C_{12} myotubes were cultured under HG conditions and then switched to LG for the indicated time to confirm that amounts of SIRT1 were reversibly controlled by ambient glucose levels (Fig. 2*F*). We also measured SIRT1 mRNA levels under these conditions and found that SIRT1 mRNA was significantly induced by switching to the LG condition ($P < 0.05$, $n = 4$; Fig. 2*G*). Thus, these results suggest that SIRT1 protein induction is regulated, at least in part, by its mRNA levels.

FoxO3a localizes in predominantly the nucleus under LG conditions but is excluded under HG conditions in C_2C_{12} myotubes. We next examined whether FoxO3a associates with the spatiotemporal changes in SIRT1 localization in response to alterations in glucose availability, since recent reports revealed functional and physical interactions between SIRT1 and FoxO transcription factors in response to various stimuli including oxidative stress (4, 36) and nutritional circumstances (38). Similar to the pattern observed in SIRT1 subcellular localization, FoxO3a was predominantly detected in the nuclei of myotubes when the cells were differentiated under LG conditions (Fig. 3*A*, *a*), whereas no nuclear localization of FoxO3 was observed in those differentiated under HG conditions (Fig. 3*A*, *c*). Again, HG administration failed to induce acute redistribution of FoxO3a (Fig. 3*B*) but resulted in a remarkable reduction of FoxO3a when the LG-differentiated myotubes (*days 5* and *6*) were exposed to HG for an additional 24 h (Fig. 3, *D* and *E*). Furthermore, we confirmed that FoxO3a protein was reversibly controlled by extracellular glucose (Fig. 3*F*) and also that FoxO3a mRNA levels were regulated by

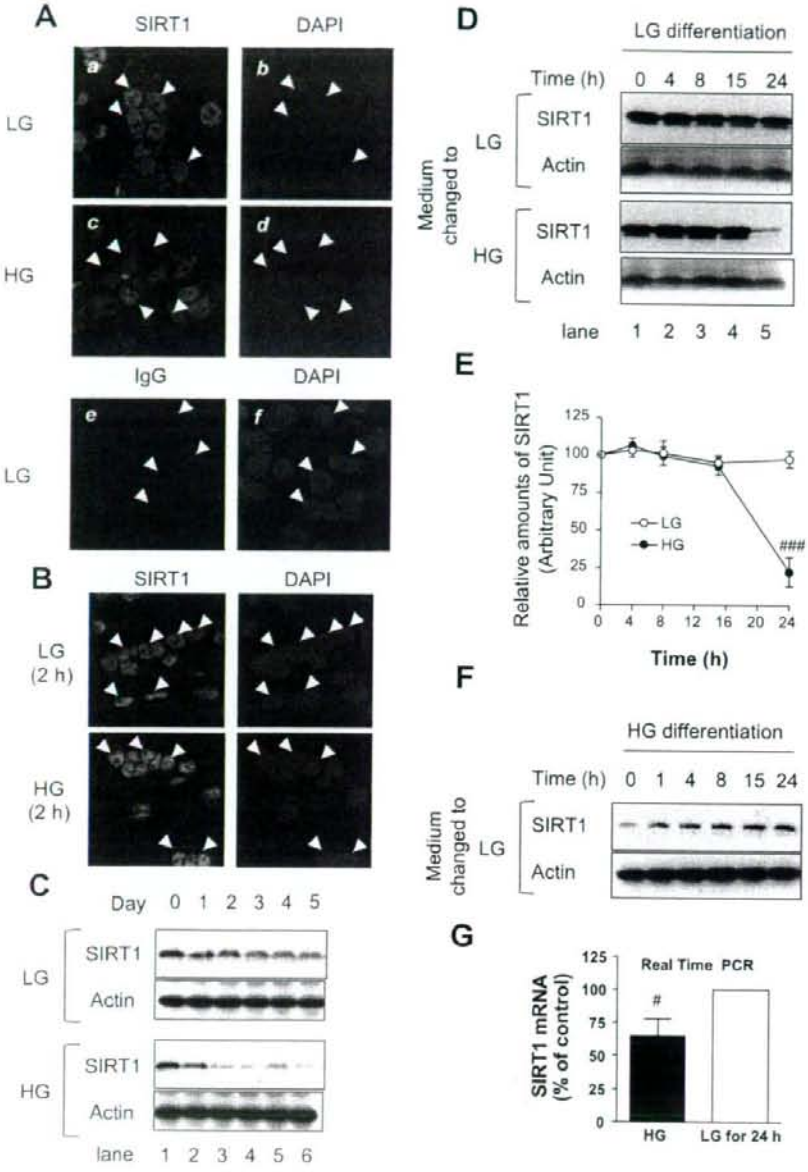

Fig. 2. Cellular abundance of SIRT1 and its localization are controlled by extracellular glucose levels during myogenesis. *A*: C_2C_{12} myoblasts were differentiated into myotubes under LG conditions (5 mM glucose in DMEM + 2% CS) or HG conditions (22.5 mM glucose in DMEM + 2% CS) for 6 days. Myotubes were then fixed and immunostained using anti-SIRT1 antibody (*a*, *c*) or anti-IgG as a negative control (*e*). DAPI staining was performed at the same time to confirm the position of the nucleus (*b*, *d*, *f*). *B*: C_2C_{12} myoblasts were differentiated into myotubes under LG conditions for 6 days. Myotubes were then incubated under LG or HG conditions for 2 h. Cells were fixed and immunostained using anti-SIRT1 antibody and DAPI. *C*: C_2C_{12} myoblasts were differentiated into myotubes under LG or HG conditions for the indicated days. Cell lysates were prepared as described in MATERIALS AND METHODS, and the same protein samples were subjected to Western blotting using anti-SIRT1 antibody. *D*: C_2C_{12} myoblasts were differentiated into myotubes under LG conditions for 6 days. Next, media were switched to LG or HG conditions, and myotubes were then further incubated for the indicated times. Cell lysates were prepared as described in MATERIALS AND METHODS, and the same protein amounts were subjected to Western blotting using anti-SIRT1 antibody. *E*: densitometric analysis of *D*. Statistical analysis was performed using 1-way ANOVA, as described in MATERIALS AND METHODS [$###P < 0.001$ vs. control (0 h), HG, $n = 3$]. *F* and *G*: C_2C_{12} myoblasts were differentiated into myotubes under HG conditions for 6 days. Next, media were switched to LG conditions, and myotubes were then further incubated for the indicated time. *F*: cell lysates were subjected to Western blotting using anti-SIRT1 antibody. *G*: total RNAs were purified and subjected to real-time PCR analysis to measure SIRT1 mRNA amounts as described in MATERIALS AND METHODS. Statistical analysis was performed using paired *t*-test ($\#P < 0.05$, $n = 3$). All experiments were performed at least 3 times, and similar results were obtained.

extracellular glucose ($P < 0.001$, $n = 4$; Fig. 3*G*). Thus, FoxO3a displayed spatiotemporal regulation similar to that observed in SIRT1 in response to altered extracellular glucose levels. However, the changes in cellular FoxO3a content during myogenesis were obviously different from those of SIRT1. As shown in Fig. 3*C*, little FoxO3a expression was observed in undifferentiated myoblasts (*day 0*), but its expression gradually increased upon differentiation only under LG conditions. This differentiation-dependent increase in the cellular content of FoxO3a was abolished when the cells were differentiated under HG conditions.

Taken together, these data demonstrate that, although acute HG treatment fails to induce subcellular redistributions of SIRT1 and FoxO3a, with chronic HG treatment (24 h) there is an obvious nuclear exclusion of these proteins concomitant with the significant reductions in their cellular contents in differentiating C_2C_{12} cells. These data also suggest the compromised myogenesis under LG conditions to be attributable to nuclear accumulation of relatively high levels of SIRT1 and FoxO3a in C_2C_{12} cells. In addition, our data indicate that 24-h exposure to HG is sufficient to produce obvious reductions in both SIRT1 and FoxO3a proteins in C_2C_{12} myotubes.

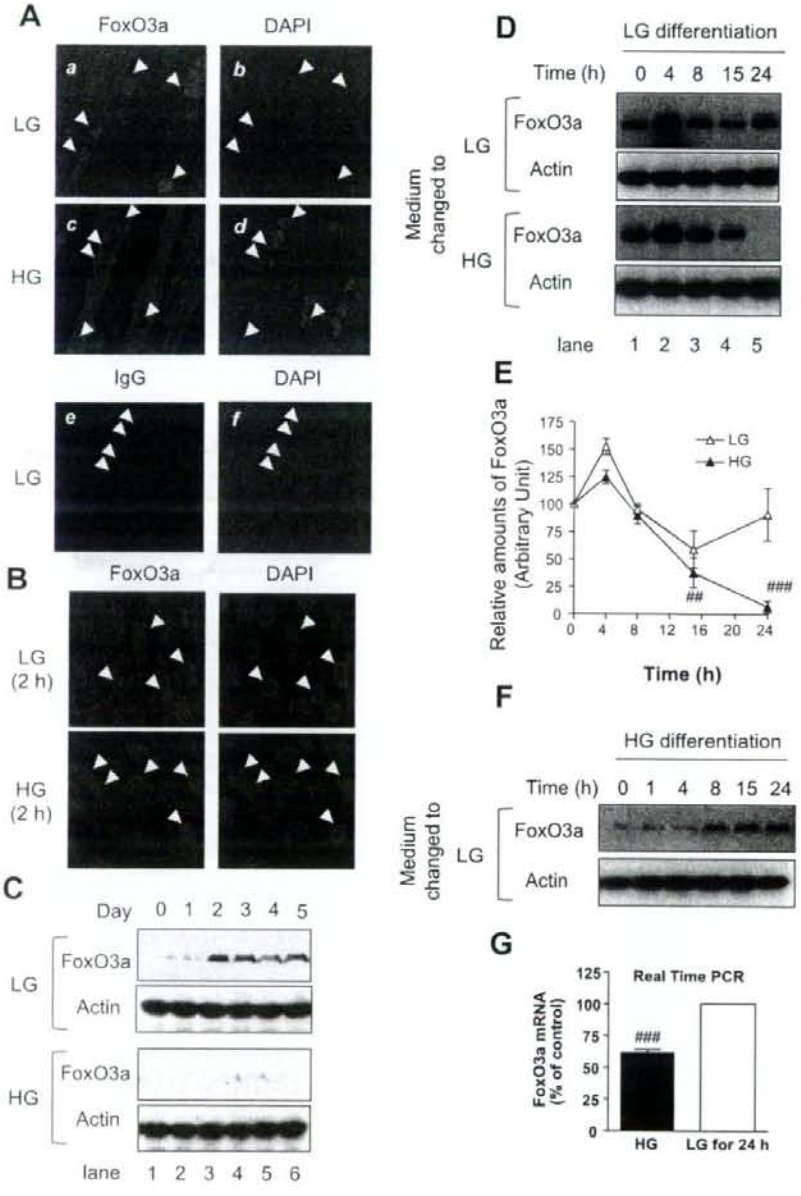

Fig. 3. Cellular abundance of FoxO3a and its localization are controlled by extracellular glucose levels during myogenesis. *A*: C_2C_{12} myoblasts were differentiated into myotubes under LG conditions (5 mM glucose in DMEM + 2% CS) or HG conditions (22.5 mM glucose in DMEM + 2% CS) for 6 days. Myotubes were then fixed and immunostained using anti-FoxO3a antibody (*a*, *c*) or anti-IgG as a negative control (*e*). DAPI staining was performed at the same time to confirm the position of the nucleus (*b*, *d*, *f*). *B*: C_2C_{12} myoblasts were differentiated into myotubes under LG conditions for 6 days. Myotubes were then incubated under LG or HG conditions for 2 h. Cells were fixed and immunostained using anti-FoxO3a antibody and DAPI. *C*: C_2C_{12} myoblasts were differentiated into myotubes under LG or HG conditions for the indicated days. Cell lysates were prepared as described in MATERIALS AND METHODS, and the same protein amounts were subjected to Western blotting analysis using anti-FoxO3a antibody. *D*: C_2C_{12} myoblasts were differentiated into myotubes under LG conditions for 6 days. Next, media were switched to LG or HG conditions, and myotubes were then further incubated for the indicated time. Cell lysates were subjected to Western blotting analysis using anti-FoxO3a antibody. *E*: densitometric analysis of *D*. Statistical analysis was performed using 1-way ANOVA followed by Tukey's posttest [##$P < 0.01$, ###$P < 0.001$, $n = 3$) vs. control (0 h, HG)]. *F* and *G*: C_2C_{12} myoblasts were differentiated into myotubes under HG conditions for 6 days. Next, media were switched to LG conditions, and myotubes were then further incubated for the indicated time. *F*: cell lysates were subjected to Western blotting using anti-FoxO3a antibody. *G*: total RNA was purified and subjected to real-time PCR analysis to measure FoxO3a mRNA amounts as described in MATERIALS AND METHODS. Statistical analysis was performed using paired *t*-test (###$P < 0.001$, $n = 3$). All experiments were performed at least 3 times, and similar results were obtained.

Extracellular glucose levels modify the stimulatory effect of insulin on myogenesis by altering cellular contents of SIRT1 and FoxO3a. Effects of HG appeared to be elicited within 24 h as assessed by the obvious reductions of both SIRT1 and FoxO3a proteins in the LG-differentiated C_2C_{12} myotubes (Figs. 2 and 3). We therefore took advantage of this phenomenon to explore the possible interplay between insulin and ambient glucose during the regulation of myogenesis. Namely, the LG-differentiated C_2C_{12} myotubes (*days 5* and *6*) were transferred to LG or HG medium in the absence or presence of the indicated insulin concentration and cultured for an additional 24 h, and the cellular contents of SIRT1 and FoxO3a were then analyzed by Western blotting (Fig. 4). In the presence of LG, insulin significantly increased cellular contents of both SIRT1 (Fig. 4*A*, *top, lanes 1–6*) and FoxO3a (Fig. 4*A*, *middle, lanes 1–6*) in a dose-dependent manner (Fig. 4, *B* and *C*, open symbols) although the amount of β-actin as a loading control was not changed (Fig. 4*A*, *bottom*). In the presence of insulin under LG conditions for 24 h, SIRT1 predominantly displayed nuclear localization, whereas increased FoxO3a displayed both cytoplasmic and nuclear localization (data not shown). In sharp contrast, insulin treatment tended to decrease

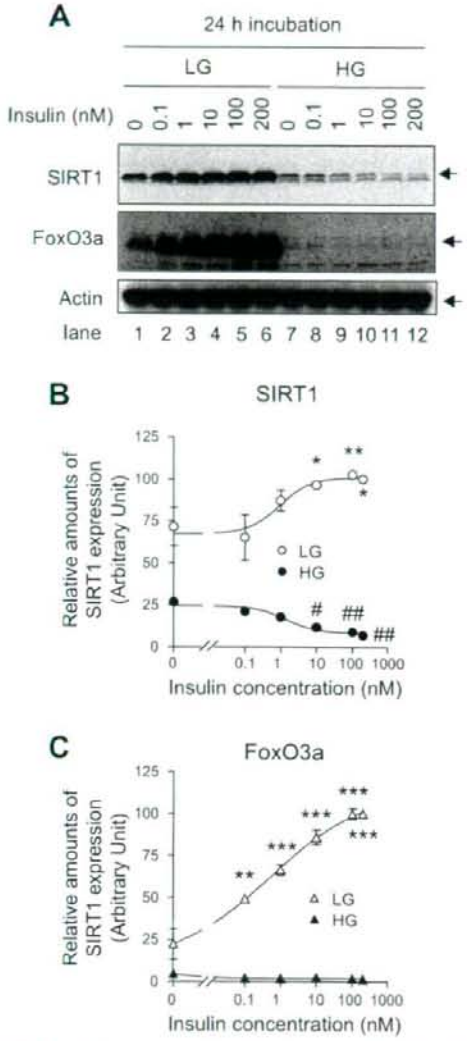

Fig. 4. Effects of insulin on SIRT1 and FoxO3a abundances depend on extracellular glucose levels. *A*: C_2C_{12} myoblasts were differentiated into myotubes under LG conditions for 6 days. Then, media were switched to HG (22.5 mM glucose in DMEM + 2% CS) or control LG (5 mM glucose in DMEM + 2% CS) in the presence or absence of the indicated concentration of insulin for 24 h. Amounts of SIRT1, FoxO3a, and β-actin were monitored by Western blotting. *B*: densitometric analysis of SIRT1 abundance during time course experiments. Statistical analysis was performed using 1-way ANOVA followed by Tukey's posttest [$^*P < 0.05$, $^{**}P < 0.01$ ($n = 3$) vs. LG control (LG, 0 nM insulin); $\#P < 0.05$, $\#\#P < 0.01$ ($n = 3$) vs. HG control (HG, 0 nM insulin)]. *C*: densitometric analysis of FoxO3a abundance during time course experiments. Statistical analysis was performed using 1-way ANOVA followed by Tukey's posttest [LG: $^*P < 0.05$, $^{**}P < 0.01$, $^{***}P < 0.001$ ($n = 3$) vs. LG control (LG, 0 nM insulin)].

SIRT1 protein in the presence of HG (Fig. 4*A*, *top*, *lanes 7–12*, and Fig. 4*B*, ●). Moreover, insulin completely failed to increase FoxO3a contents in the presence of HG (Fig. 4*A*, *bottom*, *lanes 7–12*; Fig. 4*C*, ▲). In the presence of insulin under HG conditions for 24 h, both of these proteins were barely detectable by immunofluorescent staining (data not shown).

To address the possibility that these changes in SIRT1 and FoxO3a proteins induced by the combined actions of insulin and glucose contribute to regulating the differentiation status of C_2C_{12} myotubes, the amount of MHC as a myogenic differentiation marker under each condition was also analyzed by Western blotting (Fig. 5). Consistent with the results depicted in Fig. 1, the stimulatory effect of HG on MHC expression was also detected even after incubation for just 24 h with HG (Fig. 5*A*, *lane 1* vs. *lane 6*). In the presence of HG, insulin displayed a potent myogenic-stimulating action, and MHC amounts were significantly increased in response to 100 nM insulin ($P < 0.05$, $n = 3$; Fig. 5*A*, *lanes 6–10*) under conditions in which the SIRT1 and FoxO3a contents were marginal (Fig. 4). In contrast, the myogenic stimulating potency of insulin was apparently limited (Fig. 5*A*, *lanes 1–5*) under LG conditions in which massive amounts of SIRT1 and FoxO3a were expressed (Fig. 4). The synergistic action of insulin and HG on the upregulation of MHC was clearly demonstrated by a quantitative densitometric analysis (Fig. 5*B*).

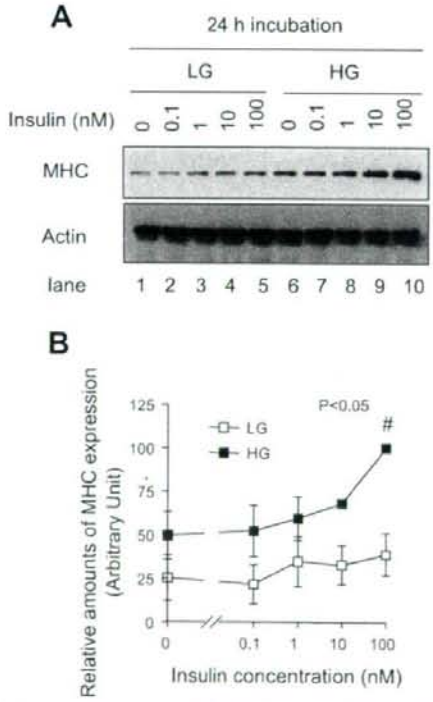

Fig. 5. Insulin myogenic potency is altered by extracellular glucose levels. *A*: C_2C_{12} myoblasts were differentiated into myotubes under LG conditions for 6 days. Then, media were switched to HG (22.5 mM glucose in DMEM + 2% CS) or control LG (5 mM glucose in DMEM + 2% CS) in the presence or absence of indicated concentration of insulin for 24 h. Amounts of myosin heavy chain (MHC) were monitored by Western blotting. *B*: densitometric analysis of *A*. Statistical analysis was performed using 1-way ANOVA followed by Tukey's posttest [HG: $\#P < 0.05$ ($n = 3$) vs. control (HG, 0 nM insulin)].

Glucose-dependent opposing effects of insulin on SIRT1 and FoxO3a are achieved through PI 3-kinase and mTOR activities. The myogenic action of insulin/IGFs has been shown to be mediated through the activation of PI 3-kinase and Akt signaling pathways (7, 23, 25, 53). In addition, several lines of evidence have demonstrated mTOR involvement in myogenesis (39, 47). To test whether the activities of PI 3-kinase and mTOR are involved in the regulation of SIRT1 and FoxO3a contents in response to insulin under LG or HG conditions, we used LY-294002 and rapamycin, potent inhibitors of PI 3-kinase and mTOR, respectively. Consistent with previous reports (8, 26, 41), the myogenic action of insulin as assessed by MHC expression, clearly detectable only in the presence of HG, was completely abolished by these compounds (Fig. 6, *A* and *C*, *bottom, lanes 4–6*). Importantly, these compounds also inhibited the insulin-mediated suppression of SIRT1 while increasing its cellular content during 24-h HG exposure (Fig. 6, *A* and *C*, *top, lanes 4–6*). Interestingly, these compounds were also effective under LG conditions and completely abolished insulin's action (Fig. 6, *A* and *C*, *middle,*

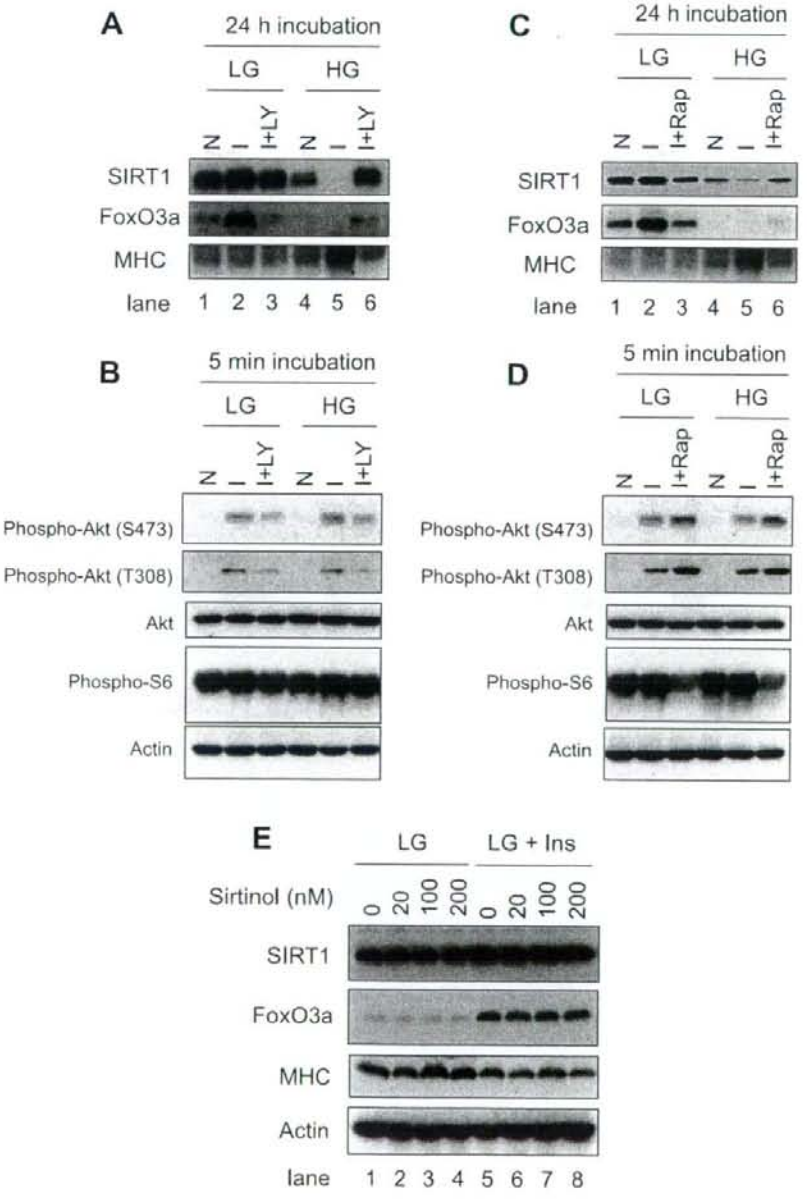

Fig. 6. Dissecting the interplay between glucose and insulin effects on SIRT1 and FoxO3a expressions and their involvements in myogenesis. *A* and *C*: C_2C_{12} myoblasts were differentiated into myotubes under LG conditions for 6 days. Media were then switched to HG or LG with or without 100 nM insulin in the presence or absence of 10 μM LY-294002 (*A*) or 50 nM rapamycin (*C*) for 24 h. Amounts of MHC, SIRT1, and FoxO3a were monitored by Western blotting. *B* and *D*: C_2C_{12} myoblasts were differentiated into myotubes under LG conditions for 6 days. Then, myotubes were treated with 100 nM insulin for 5 min in the presence or absence of 10 μM LY-294002 (*B*) or 50 nM rapamycin (*D*) under LG or HG conditions. Phosphorylations of Akt (Ser^{473} and Thr^{308}) and S6 as well as total Akt and β-actin were analyzed by Western blotting. *E*: C_2C_{12} myoblasts were differentiated into myotubes under LG conditions for 6 days. Cells were then cultured for 24 h in the presence of indicated concentrations of sirtinol under LG conditions (*lanes 1–4*) or LG + 100 nM insulin (*lanes 5–8*). Amounts of MHC, SIRT1, and FoxO3a were monitored by Western blotting. All experiments were repeated at least 3 times, and representative results are shown.

lanes 1–3), although insulin exerted completely opposing effects on the regulation of SIRT1 and FoxO3a abundances (Fig. 6, *A* and *B*, *top* and *middle*, *lane 2* vs. *lane 5*). We also monitored insulin-dependent phosphorylations of Akt and S6 in the presence of LY-294002 and rapamycin (Fig. 6, *B* and *D*). As expected, LY-294002 abolished insulin-dependent phosphorylation of Akt (Ser^{473} and Thr^{308}); on the other hand, rapamycin tended to increase insulin-dependent Akt phosphorylation (Fig. 6, *B* and *D*, *panels 1* and *2*) as previously reported (52). Phosphorylation of S6 was high under basal conditions but was slightly induced by insulin, and either LY-294002 or rapamycin had a negative effect on this phosphorylation (Fig. 6, *B and D*, *panel 4*).

Reduction of SIRT1 activity is not sufficient to restore C_2C_{12} differentiation status in the presence of insulin. Finally, we attempted to restore the poor differentiation seen under LG conditions by exposure to sirtinol, an inhibitor of SIRT1 (20, 32). Consistent with a previous study (14), 24-h exposure to sirtinol under LG conditions restored MHC expression to levels comparable to those observed in HG-exposed C_2C_{12} myotubes (Fig. 6*E*, *panel 3*, *lanes 1–4*). However, sirtinol failed to restore MHC expression (Fig. 6*E*, *panel 3*, *lanes 5–8*) in the presence of insulin, a condition in which FoxO3a is highly expressed (Fig. 6*E*, *panel 2*, *lanes 5–8*).

Changes in extracellular glucose levels during the course of overnight incubation. To precisely document the importance of ambient glucose levels in the phenomena described above, extracellular glucose concentrations were monitored during the course of overnight incubation of differentiated C_2C_{12} myotubes. As shown in Fig. 7, extracellular glucose levels gradually decreased but remained at high levels (~13 mM) even after an 18-h incubation when differentiated C_2C_{12} myotubes were cultured in HG-DMEM, whereas glucose in the medium was almost completely exhausted when the cells were cultured in LG-DMEM for 18 h.

DISCUSSION

In the present study, we demonstrated that low-serum-induced differentiation of C_2C_{12} cells is significantly influenced by extracellular glucose levels (Fig. 1), concurrently with glucose-dependent alterations in the amounts and subcellular localizations of SIRT1 and FoxO3a (Figs. 2 and 3) both of which have recently been implicated as negative regulators of myogenesis (14) (21). Consistent with many previous reports studying myogenesis by using mostly IGFs (6, 7, 12), insulin also exerts a myogenic action in a manner dependent on PI 3-kinase and mTOR activities, as assessed by MHC expression (Fig. 6); however, we cannot rule out the possibility that insulin activates IGF-I receptors since a relatively high concentration of insulin was required to stimulate MHC expression within 24 h (Fig. 5). Surprisingly, however, we found the potency of insulin's myogenic action to also be remarkably affected by extracellular glucose levels and that insulin exerts its potent myogenic effect only in the presence of relatively high levels of glucose, whereas its potency is significantly compromised in the absence of sufficient glucose (Fig. 5), perhaps due to massive increases in SIRT1 and FoxO3a, serving as negative regulators of this process, which are induced by insulin treatment under LG conditions (Figs. 4 and 6). Taken together, these results reveal an important interplay between glucose availability and insulin in the regulation of myogenesis, which is achieved, at least partially, through alterations in the cellular contents and nuclear abundances of SIRT1 and FoxO3a. Our data also document opposing effects of insulin, depending on glucose availability and thereby on the regulation of SIRT1 and FoxO3a amounts in differentiating C_2C_{12} myotubes (Fig. 6*A*). Since insulin/IGFs often display opposite biological effects, e.g., proliferation and differentiation, depending on conditions and circumstances (8, 11, 28, 30), our data presented herein provide a conceptual framework for understanding the mode of insulin actions (and presumably those of IGFs) by providing evidence that insulin's myogenic action is profoundly influenced by glucose availability mediated through regulation of SIRT1 and FoxO3a, both of which have been shown to be directly involved in the determination of cellular fates, including proliferation, differentiation, and senescence, in various cell types (1, 4, 5, 44, 50, 51).

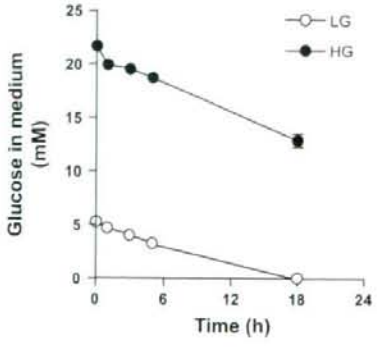

Fig. 7. Glucose consumption by C_2C_{12} myotubes. C_2C_{12} myoblasts were differentiated into myotubes for 6 days. Media were then switched to fresh medium containing LG (●) or HG (○), and glucose concentrations were measured at the indicated time.

Effects of ambient glucose levels on regulation of SIRT1 and FoxOs during myogenesis. A recent report revealed an important SIRT1 role in myogenesis by showing that overexpression of SIRT1 inhibited myogenesis, whereas either siRNA-mediated suppression of SIRT1 or sirtinol enhanced it by altering the acetylation states of MyoD and the histone acetylase p300/CBP (14). Although the SIRT1 expression level was shown to be slightly decreased upon differentiation of C_2C_{12}, the authors focused primarily on the importance of the regulation of its enzymatic activity rather than the expression level of SIRT1. In the present study, we found that SIRT1 expression is influenced by glucose levels and that SIRT1 abundance is significantly reduced in C_2C_{12} myotubes differentiated under HG conditions, a culture condition obviously potentiating myogenesis (Fig. 1). In addition, 24 h exposure of differentiating C_2C_{12} myotubes to HG (*days 5–6*) was also sufficient to decrease SIRT1 abundance (Fig. 2C), which apparently contributed to the potentiation of myogenesis as assessed by MHC expression levels (Fig. 5). Although acute redistribution was not observed with either glucose or insulin in the present study (Fig. 2B), recent reports revealed the existence of a nucleocytoplasmic shuttling mechanism for SIRT1 (24, 50). Thus, our data strongly suggest that SIRT1 abundance and its localization, being sensitively influenced by ambient glucose levels, are also directly involved in the regulation of myogenesis as a prerequisite for regulating its enzymatic activity at suitable

site(s). Consistent with this idea, a recent report demonstrated SIRT1 transcription to be regulated by metabolic states via the HIC1:CtBP corepressor complex (55). These changes in SIRT1 abundance in skeletal muscle cells may contribute not only to myogenesis but also to metabolic adaptations during glucose deprivation, such as regulation of mitochondrial gene expression and fatty acid utilization (17, 29).

Similar to what was observed in SIRT1 regulation, we found decreases in both the cellular and the nuclear abundance of FoxO3a to also be coupled to the potentiation of myogenesis, which can be induced under HG conditions (Figs. 1 and 3). These findings are consistent with a previous report showing that short interfering RNA-mediated suppression of FoxOs enhanced myogenesis, whereas its overexpression inhibited differentiation (21). Although the importance of nucleocytoplasmic shuttling of FoxOs by posttranslational modifications, such as the interplay between the Akt-mediated phosphorylation and the SIRT1-mediated deacetylation in response to growth factors and oxidative stress, is well established (3, 4), acute redistribution of FoxO3a was not detected with changes in the ambient glucose level (Fig. 3*B*), whereas its nuclear exclusion was rapidly induced by insulin, as previously reported (49). Since C_2C_{12} myocytes also express other FoxO family transcription factors, including FoxO1 and FoxO4, in addition to FoxO3a (21), our data at this stage cannot address the magnitude of the FoxO3a contribution to myogenic inhibitory action. However, our present data support previous reports showing that both SIRT1 and FoxO3a serve as negative myogenic regulators (14, 21) and also provide evidence supporting the important participation of these proteins in the process of myogenesis achieved through the regulation of their amounts and subcellular localizations. As discussed below, the physiological importance of glucose-dependent alterations in cellular SIRT1 and FoxO3a abundance in myogenesis further underscores our striking finding that insulin exerts distinct effects regulating the abundances of these proteins depending on glucose availability, which is tightly coupled with myogenic differentiation status (Fig. 4 and Fig. 5).

Interplay between ambient glucose and insulin in regulation of SIRT1 and FoxO3a and its involvement in myogenesis. In the present study, we found that the effects of ambient glucose levels can be exerted within 24 h, according to the cellular abundances of both SIRT1 and FoxO3a (Figs. 2 and 3), in differentiating C_2C_{12} myotubes. Similarly, the drastic changes in SIRT1 and FoxO abundances in various tissues, including skeletal muscle, have been reported for in vivo experiments showing that starvation increases SIRT1 and FoxOs, which are resuppressed by refeeding within 24 h (15, 16, 38, 45). In this regard, we observed that the extracellular glucose concentration falls to less than 0.5 mM after a 24-h incubation when differentiating C_2C_{12} cells are cultured in LG-DMEM (Fig. 7), even though DMEM containing 5 mM glucose (LG) is a conventional medium routinely utilized to maintain various cell types. This is probably because myotubes are postmitotic multinuclear cells that consume vast amounts of glucose as an energy source. Consequently, the cells cultured under LG conditions were perhaps experiencing an environment similar to the condition of glucose starvation, of varying degrees, during the 24-h incubation, even though the LG media were replaced daily, whereas when cells were cultured under HG conditions they were continually exposed to pathophysiologically high levels of glucose for 24 h (Fig. 7). Hence, our observations indicate that these gross culture environments, including the consequences of glucose consumption and/or exhaustion, not just the initial glucose concentration, apparently contribute to regulating SIRT1 and FoxO3a, which is in turn responsible for the modulation of myogenesis during the 24-h incubation.

One of the most intriguing observations is that insulin remarkably increases the cellular contents of both SIRT1 and FoxO3a under only LG conditions (Fig. 4*A*, *lanes 1–6*), whereas insulin completely fails to increase FoxO3a, instead decreasing the SIRT1 amount in the presence of HG (Fig. 4*A*, *lanes 7–12*). Moreover, our most striking finding is that insulin is unable to exert its myogenic action under LG conditions (Fig. 5*A*, *lanes 1–5*), whereas its potency is maximized under HG conditions, as assessed by MHC expression levels (Fig. 5*A*, *lanes 6–10*). Although it is well established that insulin and IGFs serve as potent myogenic stimulators (7, 12, 21), our present data reveal insulin's myogenic action to be significantly influenced by glucose availability. In addition, our data strongly suggest that the insulin-induced massive accumulations of these negative myogenic transcriptional regulators, SIRT1 and FoxO3a, provoked under LG conditions in differentiating C_2C_{12} myotubes counteract the myogenic stimulatory potency that insulin intrinsically possesses.

The important functional interrelationships between SIRT1 and FoxOs have been established in various organisms (18), and SIRT1 and FoxOs, including FoxO3a, have been shown to physically interact with each other to regulate their functions in a wide array of cell types (4, 10, 36). Thus, although either SIRT1 or FoxO3a alone is reportedly able to interfere with the process of myogenesis (21), it is likely that SIRT1 and FoxO3a are cooperatively involved in this interference, properly responding to alterations of culture circumstances such as glucose availability and the presence of insulin. In an attempt to evaluate the contribution of the myogenic inhibitory actions of these proteins, we utilized sirtinol to eliminate the deacetylase activity of SIRT1 and found that, although the poor differentiation state under LG conditions is significantly restored within 24 h by sirtinol (Fig. 6*C*, *bottom*, *lanes 1–4*), as previously reported (14), the sirtinol-dependent restoration of increased MHC expression is completely abolished in the presence of insulin (*lanes 5–8*). These data not only further confirm the opposing actions of insulin, i.e., that insulin can serve as a negative, rather than a positive, myogenic factor when glucose availability is low, but also suggest that the reduction of SIRT1 enzymatic activity alone might be insufficient to overcome the poor differentiation status in the presence of insulin, a condition under which FoxO3a is remarkably increased (Fig. 6*C*, *middle*, *lanes 5–8*). Thus, the considerably augmented FoxO3a may still be functional to some extent even in the presence of insulin during a 24-h incubation, which perhaps contributes to interference with the promotion of myogenesis. Moreover, since both FoxO1 and FoxO3a have been shown to increase the expressions of the ubiquitin ligases MAFbx and MuRF1, responsible for muscle atrophy via increased protein degradation (46, 49), the increased FoxO3a may also participate in the stimulation of protein degradation governed by these FoxO-inducible ubiquitin ligases. In any case, together with previous studies showing that overexpression of FoxOs results in reduced muscle mass in transgenic

mice (27) and also retards myogenesis (21), our present data suggest that the massively increased FoxO3a plays a pivotal role in exerting the inhibitory actions of insulin, at least under these experimental conditions.

Another interesting observation presented in this study is that the opposing actions of insulin depending on ambient glucose levels were both completely abolished by LY-294002 (Fig. 6*A*) or rapamycin (Fig. 6*B*). These results indicate crucial involvements of the PI 3-kinase and mTOR activities stimulated by insulin in exerting insulin actions on SIRT1 and FoxO3a depending on ambient glucose environments (Fig. 6), although the insulin-induced decrease in FoxO3a under HG conditions is not apparent due to its undetectable expression (Fig. 6, *A* and *B*, *middle, lanes 4–6*), as was the case with that observed in SIRT1 (Fig. 6, *A* and *B*, *top, lanes 4–6*). Recently, Southgate et al. (48) showed that the elevation of FoxO1 protein levels induced the nonphosphorylated form of 4EBP1, followed by reductions in Raptor and mTOR protein amounts. Together with our finding that the opposing actions of insulin on FoxO3a protein levels, which depend upon ambient glucose concentrations, are both abolished by rapamycin (Fig. 6), it is reasonable to speculate that insulin stimulates either negative or positive feedback loops on the mTOR-FoxO axis, depending on ambient glucose levels. Future work should be directed toward increasing our understanding of the mechanisms underlying the differential effects of insulin on SIRT1 and FoxOs, depending on glucose availability to solve the mystery of how insulin/IGFs exert diverse, and in some instances opposing, biological actions.

ACKNOWLEDGMENTS

We thank Fumie Wagatsuma and Natsumi Emoto for technical assistance.

GRANTS

This work was supported by Special Coordination Funds for Promoting Science and Technology. This work was also supported in part by grants from the Ministry of Education, Culture, Sports, Science and Technology of Japan and the New Energy and Industrial Technology Development Organization (NEDO).

REFERENCES

1. **Birkenkamp KU, Essafi A, van der Vos KE, da Costa M, Hui RC, Holstege F, Koenderman L, Lam EW, Coffer PJ.** FOXO3a induces differentiation of Bcr-Abl-transformed cells through transcriptional down-regulation of Id1. *J Biol Chem* 282: 2211–2220, 2007.
2. **Blander G, Guarente L.** The Sir2 family of protein deacetylases. *Annu Rev Biochem* 73: 417–435, 2004.
3. **Brunet A, Bonni A, Zigmond MJ, Lin MZ, Juo P, Hu LS, Anderson MJ, Arden KC, Blenis J, Greenberg ME.** Akt promotes cell survival by phosphorylating and inhibiting a Forkhead transcription factor. *Cell* 96: 857–868, 1999.
4. **Brunet A, Sweeney LB, Sturgill JF, Chua KF, Greer PL, Lin Y, Tran H, Ross SE, Mostoslavsky R, Cohen HY, Hu LS, Cheng HL, Jedrychowski MP, Gygi SP, Sinclair DA, Alt FW, Greenberg ME.** Stress-dependent regulation of FOXO transcription factors by the SIRT1 deacetylase. *Science* 303: 2011–2015, 2004.
5. **Chua KF, Mostoslavsky R, Lombard DB, Pang WW, Saito S, Franco S, Kaushal D, Cheng HL, Fischer MR, Stokes N, Murphy MM, Appella E, Alt FW.** Mammalian SIRT1 limits replicative life span in response to chronic genotoxic stress. *Cell Metab* 2: 67–76, 2005.
6. **Conejo R, de Alvaro C, Benito M, Cuadrado A, Lorenzo M.** Insulin restores differentiation of Ras-transformed C2C12 myoblasts by inducing NF-kappaB through an AKT/P70S6K/p38-MAPK pathway. *Oncogene* 21: 3739–3753, 2002.
7. **Conejo R, Valverde AM, Benito M, Lorenzo M.** Insulin produces myogenesis in C2C12 myoblasts by induction of NF-kappaB and down-regulation of AP-1 activities. *J Cell Physiol* 186: 82–94, 2001.
8. **Coolican SA, Samuel DS, Ewton DZ, McWade FJ, Florini JR.** The mitogenic and myogenic actions of insulin-like growth factors utilize distinct signaling pathways. *J Biol Chem* 272: 6653–6662, 1997.
9. **Cushman SW, Goodyear LJ, Pilch PF, Ralston E, Galbo H, Ploug T, Kristiansen S, Klip A.** Molecular mechanisms involved in GLUT4 translocation in muscle during insulin and contraction stimulation. *Adv Exp Med Biol* 441: 63–71, 1998.
10. **Daitoku H, Hatta M, Matsuzaki H, Aratani S, Ohshima T, Miyagishi M, Nakajima T, Fukamizu A.** Silent information regulator 2 potentiates Foxo1-mediated transcription through its deacetylase activity. *Proc Natl Acad Sci USA* 101: 10042–10047, 2004.
11. **Ewton DZ, Florini JR.** Effects of the somatomedins and insulin on myoblast differentiation in vitro. *Dev Biol* 86: 31–39, 1981.
12. **Florini JR, Ewton DZ, Coolican SA.** Growth hormone and the insulin-like growth factor system in myogenesis. *Endocr Rev* 17: 481–517, 1996.
13. **Fujita H, Nedachi T, Kanzaki M.** Accelerated de novo sarcomere assembly by electric pulse stimulation in C2C12 myotubes. *Exp Cell Res* 313: 1853–1865, 2007.
14. **Fulco M, Schiltz RL, Iezzi S, King MT, Zhao P, Kashiwaya Y, Hoffman E, Veech RL, Sartorelli V.** Sir2 regulates skeletal muscle differentiation as a potential sensor of the redox state. *Mol Cell* 12: 51–62, 2003.
15. **Furuyama T, Kitayama K, Yamashita H, Mori N.** Forkhead transcription factor FOXO1 (FKHR)-dependent induction of PDK4 gene expression in skeletal muscle during energy deprivation. *Biochem J* 375: 365–371, 2003.
16. **Furuyama T, Yamashita H, Kitayama K, Higami Y, Shimokawa I, Mori N.** Effects of aging and caloric restriction on the gene expression of Foxo1, 3, and 4 (FKHR, FKHRL1, and AFX) in the rat skeletal muscles. *Microsc Res Tech* 59: 331–334, 2002.
17. **Gerhart-Hines Z, Rodgers JT, Bare O, Lerin C, Kim SH, Mostoslavsky R, Alt FW, Wu Z, Puigserver P.** Metabolic control of muscle mitochondrial function and fatty acid oxidation through SIRT1/PGC-1alpha. *EMBO J* 26: 1913–1923, 2007.
18. **Giannakou ME, Partridge L.** The interaction between FOXO and SIRT1: tipping the balance towards survival. *Trends Cell Biol* 14: 408–412, 2004.
19. **Gotta M, Strahl-Bolsinger S, Renauld H, Laroche T, Kennedy BK, Grunstein M, Gasser SM.** Localization of Sir2p: the nucleolus as a compartment for silent information regulators. *EMBO J* 16: 3243–3255, 1997.
20. **Grozinger CM, Chao ED, Blackwell HE, Moazed D, Schreiber SL.** Identification of a class of small molecule inhibitors of the sirtuin family of NAD-dependent deacetylases by phenotypic screening. *J Biol Chem* 276: 38837–38843, 2001.
21. **Hribal ML, Nakae J, Kitamura T, Shutter JR, Accili D.** Regulation of insulin-like growth factor-dependent myoblast differentiation by Foxo forkhead transcription factors. *J Cell Biol* 162: 535–541, 2003.
22. **Jiang BH, Aoki M, Zheng JZ, Li J, Vogt PK.** Myogenic signaling of phosphatidylinositol 3-kinase requires the serine-threonine kinase Akt/protein kinase B. *Proc Natl Acad Sci USA* 96: 2077–2081, 1999.
23. **Jiang BH, Zheng JZ, Vogt PK.** An essential role of phosphatidylinositol 3-kinase in myogenic differentiation. *Proc Natl Acad Sci USA* 95: 14179–14183, 1998.
24. **Jin Q, Yan T, Ge X, Sun C, Shi X, Zhai Q.** Cytoplasm-localized SIRT1 enhances apoptosis. *J Cell Physiol* 213: 88–97, 2007.
25. **Kaliman P, Canicio J, Shepherd PR, Beeton CA, Testar X, Palacin M, Zorzano A.** Insulin-like growth factors require phosphatidylinositol 3-kinase to signal myogenesis: dominant negative p85 expression blocks differentiation of L6E9 muscle cells. *Mol Endocrinol* 12: 66–77, 1998.
26. **Kaliman P, Vinals F, Testar X, Palacin M, Zorzano A.** Phosphatidylinositol 3-kinase inhibitors block differentiation of skeletal muscle cells. *J Biol Chem* 271: 19146–19151, 1996.
27. **Kamei Y, Miura S, Suzuki M, Kai Y, Mizukami J, Taniguchi T, Mochida K, Hata T, Matsuda J, Aburatani H, Nishino I, Ezaki O.** Skeletal muscle FOXO1 (FKHR) transgenic mice have less skeletal muscle mass, down-regulated type I (slow twitch/red muscle) fiber genes, and impaired glycemic control. *J Biol Chem* 279: 41114–41123, 2004.
28. **Kanzaki M, Hattori M, Kojima I.** Growth or differentiation: determination by FSH of the action of insulin-like growth factor-I in cultured rat granulosa cells. *Endocr J* 43: 15–23, 1996.
29. **Lagouge M, Argmann C, Gerhart-Hines Z, Meziane H, Lerin C, Daussin F, Messadeq N, Milne J, Lambert P, Elliott P, Geny B, Laakso M, Puigserver P, Auwerx J.** Resveratrol improves mitochondrial

function and protects against metabolic disease by activating SIRT1 and PGC-1alpha. *Cell* 127: 1109–1122, 2006.

30. **Lorenzo M, Valverde AM, Teruel T, Benito M.** IGF-I is a mitogen involved in differentiation-related gene expression in fetal rat brown adipocytes. *J Cell Biol* 123: 1567–1575, 1993.
31. **Lu J, McKinsey TA, Zhang CL, Olson EN.** Regulation of skeletal myogenesis by association of the MEF2 transcription factor with class II histone deacetylases. *Mol Cell* 6: 233–244, 2000.
32. **Luo J, Nikolaev AY, Imai S, Chen D, Su F, Shiloh A, Guarente L, Gu W.** Negative control of p53 by Sir2alpha promotes cell survival under stress. *Cell* 107: 137–148, 2001.
33. **McKinsey TA, Zhang CL, Lu J, Olson EN.** Signal-dependent nuclear export of a histone deacetylase regulates muscle differentiation. *Nature* 408: 106–111, 2000.
34. **Michishita E, Park JY, Burneskis JM, Barrett JC, Horikawa I.** Evolutionarily conserved and nonconserved cellular localizations and functions of human SIRT proteins. *Mol Biol Cell* 16: 4623–4635, 2005.
35. **Molkentin JD, Black BL, Martin JF, Olson EN.** Cooperative activation of muscle gene expression by MEF2 and myogenic bHLH proteins. *Cell* 83: 1125–1136, 1995.
36. **Motta MC, Divecha N, Lemieux M, Kamel C, Chen D, Gu W, Bultsma Y, McBurney M, Guarente L.** Mammalian SIRT1 represses forkhead transcription factors. *Cell* 116: 551–563, 2004.
37. **Nedachi T, Kanzaki M.** Regulation of glucose transporters by insulin and extracellular glucose in C_2C_{12} myotubes. *Am J Physiol Endocrinol Metab* 291: E817–E828, 2006.
38. **Nemoto S, Fergusson MM, Finkel T.** Nutrient availability regulates SIRT1 through a forkhead-dependent pathway. *Science* 306: 2105–2108, 2004.
39. **Park IH, Chen J.** Mammalian target of rapamycin (mTOR) signaling is required for a late-stage fusion process during skeletal myotube maturation. *J Biol Chem* 280: 32009–32017, 2005.
40. **Picard F, Kurtev M, Chung N, Topark-Ngarm A, Senawong T, Machado De Oliveira R, Leid M, McBurney MW, Guarente L.** Sirt1 promotes fat mobilization in white adipocytes by repressing PPAR-gamma. *Nature* 429: 771–776, 2004.
41. **Pinset C, Garcia A, Rousse S, Dubois C, Montarras D.** Wortmannin inhibits IGF-dependent differentiation in the mouse myogenic cell line C2. *C R Acad Sci III* 320: 367–374, 1997.
42. **Pownall ME, Gustafsson MK, Emerson CP Jr.** Myogenic regulatory factors and the specification of muscle progenitors in vertebrate embryos. *Annu Rev Cell Dev Biol* 18: 747–783, 2002.
43. **Puri PL, Iezzi S, Stiegler P, Chen TT, Schiltz RL, Muscat GE, Giordano A, Kedes L, Wang JY, Sartorelli V.** Class I histone deacetylases sequentially interact with MyoD and pRb during skeletal myogenesis. *Mol Cell* 8: 885–897, 2001.
44. **Qiao L, Shao J.** SIRT1 regulates adiponectin gene expression through Foxo1-C/enhancer-binding protein alpha transcriptional complex. *J Biol Chem* 281: 39915–39924, 2006.
45. **Rodgers JT, Lerin C, Haas W, Gygi SP, Spiegelman BM, Puigserver P.** Nutrient control of glucose homeostasis through a complex of PGC-1alpha and SIRT1. *Nature* 434: 113–118, 2005.
46. **Sandri M, Sandri C, Gilbert A, Skurk C, Calabria E, Picard A, Walsh K, Schiaffino S, Lecker SH, Goldberg AL.** Foxo transcription factors induce the atrophy-related ubiquitin ligase atrogin-1 and cause skeletal muscle atrophy. *Cell* 117: 399–412, 2004.
47. **Shu L, Zhang X, Houghton PJ.** Myogenic differentiation is dependent on both the kinase function and the N-terminal sequence of mammalian target of rapamycin. *J Biol Chem* 277: 16726–16732, 2002.
48. **Southgate RJ, Neill B, Prelovsek O, El-Osta A, Kamei Y, Miura S, Ezaki O, McLoughlin TJ, Zhang W, Unterman TG, Febbraio MA.** FOXO1 regulates the expression of 4E-BP1 and inhibits mTOR signaling in mammalian skeletal muscle. *J Biol Chem* 282: 21176–21186, 2007.
49. **Stitt TN, Drujan D, Clarke BA, Panaro F, Timofeyva Y, Kline WO, Gonzalez M, Yancopoulos GD, Glass DJ.** The IGF-1/PI3K/Akt pathway prevents expression of muscle atrophy-induced ubiquitin ligases by inhibiting FOXO transcription factors. *Mol Cell* 14: 395–403, 2004.
50. **Tanno M, Sakamoto J, Miura T, Shimamoto K, Horio Y.** Nucleocytoplasmic shuttling of the NAD+-dependent histone deacetylase SIRT1. *J Biol Chem* 282: 6823–6832, 2007.
51. **van der Horst A, Tertoolen LG, de Vries-Smits LM, Frye RA, Medema RH, Burgering BM.** FOXO4 is acetylated upon peroxide stress and deacetylated by the longevity protein hSir2 (SIRT1). *J Biol Chem* 279: 28873–28879, 2004.
52. **Wan X, Harkavy B, Shen N, Grohar P, Helman LJ.** Rapamycin induces feedback activation of Akt signaling through an IGF-1R-dependent mechanism. *Oncogene* 26: 1932–1940, 2007.
53. **Xu Q, Wu Z.** The insulin-like growth factor-phosphatidylinositol 3-kinase-Akt signaling pathway regulates myogenin expression in normal myogenic cells but not in rhabdomyosarcoma-derived RD cells. *J Biol Chem* 275: 36750–36757, 2000.
54. **Yaffe D, Saxel O.** Serial passaging and differentiation of myogenic cells isolated from dystrophic mouse muscle. *Nature* 270: 725–727, 1977.
55. **Zhang Q, Wang SY, Fleuriel C, Leprince D, Rocheleau JV, Piston DW, Goodman RH.** Metabolic regulation of SIRT1 transcription via a HIC1:CtBP corepressor complex. *Proc Natl Acad Sci USA* 104: 829–833, 2007.

THE JOURNAL OF BIOLOGICAL CHEMISTRY VOL. 283, NO. 15, pp. 10208–10220, April 11, 2008

Functional Role of Sortilin in Myogenesis and Development of Insulin-responsive Glucose Transport System in C2C12 Myocytes*

Received for publication, December 31, 2007 Published, JBC Papers in Press, February 7, 2008, DOI 10.1074/jbc.M710604200

Miyako Ariga[‡§¶1], **Taku Nedachi**[§], **Hideki Katagiri**[‡¶], **and Makoto Kanzaki**[§2]

From the [‡]*21st Century COE program Comprehensive Research and Education Center for Planning of Drug Development and Clinical Evaluation, Graduate School of Pharmaceutical Sciences, Tohoku University, Sendai 980-8575, the* [§]*Division of Biomaterials, Biomedical Engineering Research Organization, Tohoku University, 2-1 Seiryo-machi, Aoba-ku, Sendai 980-8575, and the* [¶]*Division of Advanced Therapeutics for Metabolic Diseases, Center for Translational and Advanced Animal Research, Tohoku University Graduate School of Medicine, Sendai 980-8575, Japan*

Sortilin has been implicated in the formation of insulin-responsive GLUT4 storage vesicles in adipocytes by regulating sorting events between the *trans*-Golgi-network and endosomes. We herein show that sortilin serves as a potent myogenic differentiation stimulator for C2C12 myocytes by cooperatively functioning with p75NTR, which subsequently further contributes to development of the insulin-responsive glucose transport system in C2C12 myotubes. Sortilin expression was up-regulated upon C2C12 differentiation, and overexpression of sortilin in C2C12 cells significantly stimulated myogenic differentiation, a response that was completely abolished by either anti-p75NTR- or anti-nerve growth factor (NGF)-neutralizing antibodies. Importantly, small interference RNA-mediated suppression of endogenous sortilin significantly inhibited C2C12 differentiation, indicating the physiological significance of sortilin expression in the process of myogenesis. Although sortilin overexpression in C2C12 myotubes improved insulin-induced 2-deoxyglucose uptake, as previously reported, this effect apparently resulted from a decrease in the cellular content of GLUT1 and an increase in GLUT4 via differentiation-dependent alterations at both the gene transcriptional and the post-translational level. In addition, cellular contents of Ubc9 and SUMO-modified proteins appeared to be increased by sortilin overexpression. Taken together, these data demonstrate that sortilin is involved not only in development of the insulin-responsive glucose transport system in myocytes, but is also directly involved in muscle differentiation via modulation of proNGF-p75NTR.

One of the major physiological roles of insulin is the control of postprandial blood glucose levels, and skeletal muscle is the primary tissue responsible for the bulk (70–80%) of insulin-stimulated postprandial glucose disposal (1, 2). The effect of insulin on overall glucose disposal is primarily achieved via stimulation of glucose uptake into insulin-target tissues, and defects in this insulin action in skeletal muscle contribute to development of the insulin resistance which is characteristic of type 2 diabetes (3).

In skeletal muscle, glucose transport is regulated by a facilitative glucose transport system involving at least two members of the glucose transporter family, GLUT1 and GLUT4 (4), and their expression levels are strictly regulated during myocyte differentiation (5, 6). GLUT1 is targeted predominantly to the sarcolemma (muscle plasma membrane) and is therefore implicated in the regulation of basal glucose transport, although a marked reduction in GLUT1 expression occurs during muscle differentiation (5, 6). In contrast, expression of the insulin-responsive glucose transporter GLUT4 is remarkably up-regulated upon muscle differentiation, and GLUT4 protein is predominantly localized in intracellular tubulo-vesicular elements under basal conditions (7, 8), while insulin stimulates the translocation of GLUT4 from intracellular storage compartments to the cell surface, resulting in the insulin-responsive augmentation of glucose uptake (9). Thus, differentiation-dependent changes in the amount and composition of these GLUT proteins, especially the increase in cellular GLUT4 content, contribute to development of the insulin-responsive glucose transport system in myocytes and adipocytes (5, 10). However, GLUT4 expression is not the only factor responsible for conferring the insulin-stimulated glucose uptake function in these insulin-responsive cells, because ectopic expression of GLUT4 in other cell types such as fibroblasts is insufficient to generate an insulin-stimulated glucose transport system (11, 12).

Recent studies using adipocytes have revealed that one of the additional factors prerequisite for higher insulin responsiveness is a signaling cascade developed during the course of adipocyte differentiation that is absent in pre-adipocytes (13, 14). In addition to differentiation-dependent establishment of this signaling cascade, Kandror and colleagues (15, 16) recently reported that sortilin, a type I transmembrane glycoprotein, which is implicated in the sorting of Vps10p-interacting proteins between the *trans*-Golgi network, plasma membrane, and lysosomes, serves as another important factor that promotes development of the insulin-induced glucose transport system

* This work was supported in part by grants from the New Energy and Industrial Technology Development Organization and the Ministry of Education, Science, Sports and Culture of Japan. The costs of publication of this article were defrayed in part by the payment of page charges. This article must therefore be hereby marked "*advertisement*" in accordance with 18 U.S.C. Section 1734 solely to indicate this fact.

[1] Supported by Research Fellowships of the Japan Society for the Promotion of Science for Young Scientists.

[2] Supported by Special Coordinated Funds for Promoting Science and Technology. To whom correspondence should be addressed: Tel.: 81-22-717-7581; Fax: 81-22-717-7578; E-mail: kanzakimakoto@mac.com.

by producing insulin-responsive GLUT4 storage vesicles. They found that fibroblasts ectopically expressing both sortilin and GLUT4 display significantly augmented glucose uptake in response to insulin stimulation (12). Although it has already been reported that sortilin is expressed in muscle (17, 18), at present the functional role of sortilin in muscle is entirely unknown, although muscle is the tissue in which the insulin effect on postprandial glucose disposal is quantitatively most important.

Sortilin was originally purified from human brain extracts using receptor-associated protein affinity chromatography (17) and was also identified as a major component of GLUT4-containing vesicles from rat adipocytes (18, 19). Sortilin has a Vps10p domain in its luminal region at the N terminus and therefore belongs to the mammalian VPS10p family of sorting receptors. The intraluminal domain of sortilin was shown to interact with a wide array of proteins, including an unprocessed form of nerve growth factor (proNGF),[3] neurotensin, lipoprotein lipase, precursor of brain-derived neurotrophic factor (BDNF), and prosaposin, as well as receptor-associated protein (16, 17, 20–23). Therefore, sortilin functions not only to direct the intracellular movements of such newly synthesized interacting proteins but also functions as a receptor for these proteins once sortilin is exposed to the cell surface plasma membrane. Nevertheless, the cytoplasmic tail of sortilin does not possess a domain enabling it to directly activate the intracellular signaling cascade (24). Recent studies have, however, revealed that sortilin forms a complex with proNGF and p75NTR, a low affinity NGF receptor, and triggers p75NTR signaling cascades leading to various cellular responses, including differentiation, survival, and apoptosis (22, 25). Interestingly, genes encoding precursors of NGF and BDNF, and their common low affinity receptor p75NTR, were shown to be expressed in C2C12 myoblasts (26). In addition, several lines of evidence indicate that NGF affects myogenic differentiation and muscle development in an autocrine fashion via p75NTR (26–28).

In the present study, we explored the functional roles of sortilin in muscle by using the skeletal muscle cell line C2C12. We herein report sortilin to be a potent differentiation stimulator functioning cooperatively with p75NTR, which subsequently further contributes to development of the insulin responsive glucose transport system in C2C12 cells. We present compelling evidence that sortilin is involved not only in generating insulin-responsive GLUT4 storage vesicles but also in elaborating an entire glucose transport system exhibiting much higher insulin responsiveness via regulation of the processes of myogenesis, including expressions of GLUT proteins and perhaps various other proteins involved in the development of insulin responsiveness. Thus, our results provide new insights into the functional roles of sortilin in myogenesis and in development of the insulin-responsive glucose transport system in myocytes.

[3] The abbreviations used are: proNGF, unprocessed form of nerve growth factor; NGF, nerve growth factor; p75NTR, p75 neurotrophin receptor; Vps, vacuolar protein sorting; GGA, Golgi-localizing γ-adaptin ear homology domain, ARF-binding proteins; ARF, ADP-ribosylation factor; siRNA, small interfering RNA; SUMO, small ubiquitin-related modifier; BDNF, brain-derived neurotrophic factor; MHC, myosin heavy chain; DMEM, Dulbecco's modified Eagle's medium; BSA, bovine serum albumin; ECFP, enhanced cyan fluorescent protein; PBS, phosphate-buffered saline; Ab, antibody.

EXPERIMENTAL PROCEDURES

Materials—We obtained 2-deoxy-[^{3}H]glucose (37.2 Ci/mmol) from PerkinElmer Life Sciences. The Western blot detection kit (West super femto detection reagents) was from Pierce. Dulbecco's Modified Eagle Medium (DMEM), penicillin/streptomycin and Trypsin-EDTA were purchased from Sigma. Cell culture equipment was from BD Biosciences (San Jose, CA). Calf serum and fetal bovine serum were obtained from BioWest (Nuaille, France). Immobilon-P was from Millipore Corp. (Bedford, MA). Bovine serum albumin (BSA) was purchased from Wako (Osaka, Japan). Antibodies against sortilin, p115, syntaxin 6, Ubc9, and SUMO-modified protein 1 (GMP1) were purchased from BD Biosciences. Anti-sortilin antibody obtained from Abcam (Cambridge, UK) was used for immunofluorescent analyses. Antibodies against cation-independent mannose 6-phosphate/insulin-like growth factor-2 receptor, insulin receptor β-subunit, and c-Myc (9E10) were purchased from Santa Cruz Biotechnology (Santa Cruz, CA). Anti-myosin heavy chain (MHC) (MF20), anti-myogenin (F5D), anti-troponin T (CT3), and anti-titin (9D10) antibodies were obtained from Iowa Hybridoma Bank (University of Iowa, Iowa City, IA). Anti-sarcomeric α-actinin (EA-53) and anti-β-actin (A-2066) antibodies were purchased from Sigma. Anti-GLUT1 antibody was purchased from Chemicon International Inc. (Temecula, CA). Anti-p75NTR antibody (ME20.4) was obtained from Abcam. Anti-GLUT4 antibody was a generous gift from Dr. H. Shibata (Gunma University, Maebashi, Japan) (29). Fluorescence-conjugated secondary antibodies were obtained from Invitrogen. Unless otherwise noted, all chemicals were of the purest grade available from Sigma Chemicals.

Cell Culture—Myoblasts from the mouse skeletal muscle cell line C2C12 (30) were maintained in DMEM supplemented with 10% fetal bovine serum, 30 mg/ml penicillin, and 100 mg/ml streptomycin (growth medium) at 37 °C under a 5% CO_2 atmosphere. For biochemical study, cells were grown on 6-well plates (BD Biosciences) at a density of 3×10^4 cells/well in 3 ml of growth medium. Three days after plating, the cells had reached ~80–90% confluence (Day 0). Differentiation was then induced by switching the growth medium to DMEM supplemented with 2% calf serum, 30 μg/ml penicillin, and 100 μg/ml streptomycin (differentiation medium). The differentiation medium was changed every 24 h. For the immunofluorescent staining study, cells were grown on 22-mm glass coverslips (Matsunami C022221, Osaka, Japan) in 6-well plates.

Generation of C2C12 Cells Expressing Sortilin—Human sortilin cDNA was inserted into a pMXs retroviral vector, which is generated by modifying the pBABE retroviral vector (31). The pMXs-sortilin or pMXs (control) was transfected into Plat E cells using FuGENE 6 transfection reagents (Roche Applied Science, Indianapolis, IN), and high titer retroviral supernatants were obtained. C2C12 myoblasts were infected with the generated retrovirus in growth medium containing 10 μg/ml Polybrene. Two days after infection, positive selection was performed in the presence of 5 μg/ml puromycin, and 20 individual clones were isolated. The sortilin expression level in